# Dry-Processable Carbon Nanotubes for Functional Devices and Composites

*Jiangtao Di, Xin Wang, Yajuan Xing, Yongyi Zhang, Xiaohua Zhang, Weibang Lu, Qingwen Li,* and Yuntian T. Zhu**


## From the Contents



*Assembly of carbon nanotubes (CNTs) in effective and productive ways is of vital importance to their application. Recent progress in synthesis of CNTs has inspired new strategies for utilizing the unique physiochemical properties of CNTs in macroscale materials and devices. Assembling CNTs by dry processes (e.g., directly collecting CNTs in the form of freestanding films followed by pressing, stretching, and multilayer stacking instead of dispersing them in solution) not only considerably simplifies the processes but also avoids structural damage to the CNTs. Various dry-processable CNTs are reviewed, focusing on their synthesis, properties, and applications. The synthesis techniques are organized in terms of aggregative morphologies and microstructure control of CNTs. Important applications such as functional thin-film devices, strong CNT films, and composites are included. The opportunities and challenges in the synthesis techniques and fabrication of advanced composites and devices are discussed.*

NANO MICRO small

## 1. Introduction

Carbon nanotubes (CNTs) have been expected to be applicable in diverse areas, such as electronics, aerospace, automotive, chemistry and biomedical engineering,[1] because of their superior mechanical properties (100–200 GPa in tensile strength and ~1 TPa in modulus when calculated considering the cross-sectional area of CNT walls),[2] thermal conductivity (experimentally measured as up to 3000 W $m^{-1}$ $K^{-1}$),[3] and electrical properties. It has been realized that all of the applications strongly rely on how to assemble CNTs efficienctly to form macroscale materials and devices with the best utilization of the unique physiochemical properties of CNTs.[4] Currently, wet chemistry methods are widely used for processing CNTs in which nanotubes are purified (removal of catalyst and amorphous carbon), dispersed, and assembled with the aid of solutions.[5] Although they are applicable to most of raw nanotubes, structural damage to CNTs are inevitable,[6] such as scission of nanotubes, $sp^2$ bond breakage, and contamination. In addition, the dissolution and/or surface functionalization by strong acids and/or other chemical solutions are environmentally problematic and time-consuming.

The emergence of CNTs that can be processed in dry-state (hereafter referred to as dry-processable CNTs) provides a straightforward route for assembling CNT with different orientation, density and inter-tube connections. As shown in **Table 1**, the dry-processing methods have the advantage of avoiding complex and time-consuming processes that are typical for solution-based methods. Dry-processable CNTs typically self-assemble into novel structures during chemical vapor deposition processes. This means that they are ready for some applications without involving complex solution processes. For example, CNT arrays (also called forests) grown vertically on silicon substrates have an aligned structure that is ideal for thermal interface management,[7] and electrodes of supercapacitors and batteries.[8] By tuning the packing density and alignment of CNTs, transparent and conducting CNT sheets have been continuously drawn from vertical CNT arrays,[9] which have potential for many applications.[10] In addition, dry-processable CNTs can retain most of their novel intrinsic properties such as large length-to-diameter ratio and high electrical and thermal conductivity because of no structure damage involved in dry processes. Therefore, they can be expected to have high performances as shown by the comparison results in **Table 2**. For example, macroscopic films assembled from dry-processable CNTs exhibited strength and modulus several times higher than the films prepared by wet chemistry methods.[11] Similarly, fibers spun from dry-processable CNTs show much better mechanical performance than those from the solution methods as summarized in a recent review by Lu et al.[12] Devices such as solar cells, supercapacitors, lithium ion batteries, touch screen, and loudspeakers that use dry-processable CNTs as electrodes also exhibit superior performance.

This review focuses on the dry processable CNTs, including nanotube synthesis from the viewpoints of assembly morphologies and structure control of CNTs and their novel applications such as strong composites and functional devices. We will also discuss the opportunities and challenges of dry processable CNTs.

## 2. Approaches for Growing Dry-Processable CNTs

Dry-processable CNTs can be prepared by tailoring the growth and aggregate morphology of CNTs during chemical vapor deposition. For example, uniformly distributing catalytic nanoparticles on silicon substrates can help with growing vertically aligned nanotube arrays (or forests),[13] while floating catalytic nanoparticles in the flowing gas can lead to interwoven CNT webs or yarns formed inside of the reactor zone, which is further collected downstream of a furnace.[14] Particularly, the later method is known as floating catalytic chemical vapor deposition (FCCVD), which is modified from a method previously developed for preparing carbon nanofibers.[15]

### 2.1. Floating Catalyst Chemical Vapor Deposition

In typical FCCVD processes,[14a] catalyst-containing compounds such as ferrocene and iron pentacarbonyl are dissolved in a carbon source solution such as benzene, ethanol and methanol and then fed into a CNT growth reactor. The catalyst solution vaporizes at the low temperature zone (~200 °C) and feeds into the high temperature zone of a reactor, together with flowing forming gas such as diluted hydrogen. The decomposition of the precursor compound produces catalyst nanoparticles, which catalytically decompose carbon sources. CNTs nucleate on the catalyst nanoparticles and grow after carbon becomes saturated. During this process, catalysts and CNTs float in forming gas and move with gas flow. Finally, CNT films deposit at the end zone of the reactor. A small amount of sulfur-containing additive, for example thiophene, is usually added to enhance the nanotube growth.[14a]

The floating method has produced various CNT assemblies. Historically, Cheng and co-workers reported in 1998 the synthesis of bulk single-walled carbon nanotubes

Dr. J. Di,[+] Dr. Y. Xing, Dr. Y. Zhang,
Dr. X. Zhang, Prof. W. Lu, Prof. Q. Li
Suzhou Institute of Nano-tech and Nano-bionics
Chinese Academy of Sciences
Suzhou 215123, China
E-mail: qwli2007@sinano.ac.cn

Dr. X. Wang, Prof. Y. T. Zhu
Department of Materials Science and Engineering
North Carolina State University
Raleigh, NC 27695, USA
E-mail: ytzhu@ncsu.edu

Prof. Y. T. Zhu
School of Materials Science and Engineering
Nanjing University of Science and Technology
Nanjing 210094, China

[+]*Present Address:* The Alan G. MacDiarmid NanoTech Institute, University of Texas at Dallas, Richardson, TX 75083, USA

DOI: 10.1002/smll.201401465

  

(SWCNTs).[16] CNTs self-organized into a random form and entangled into an irregular bulk assembly as shown in **Figure 1**A. The CNT assembly contained impurities such as multi-walled carbon nanotubes (MWCNTs), amorphous carbon, and catalysts. The purity was about 60% in mass. Song and co-workers reported the synthesis of a film-like SWCNT assembly.[17] Instead of dissolving catalysts in a solution as in Cheng's method, they put the catalyst powder in a chamber close to the gas inlet, and the catalyst particles were sublimed and brought into the reaction zone by argon and methane.[17] Liu et al. modified Cheng's method by designing a porous membrane fixed at the outlet of the quartz reaction tube as a substrate to collect nanotube films and prepared book-like SWCNT assemblies (also called "buckybooks").[18] As shown in Figure 1B, a nanotube buckybook consisted of several hundreds of homogeneous thin monosheets with a thickness of ~500 nm. Interestingly, CNT monosheets could be readily peeled off from the buckybook, which was semi-transparent and conductive (Figure 1C). Similarly, Ma and co-workers reported that a transparent SWCNT film could be collected on a rolling plate that was placed at the downstream of the reactant gases in a FCCVD furnace.[19] After peeling it off from the plate, the film was freestanding, conductive and mechanically robust with a tensile strength of 360 MPa. The film can serve as transparent electrodes or precursor for nanotube yarns. Li and co-workers further advanced FCCVD for continuous synthesis of CNT films or fibers.[14b] They intentionally employed a mechanical tool to draw as-formed nanotubes out of the furnace as schematically shown in Figure 1D. The key requirements for the continuous synthesis were the rapid formation of CNT aerogels in the furnace and the forcible removal of the aerogel by continuous wind-up. In their system, they used a vertical hot furnace system and they fed the catalyst solution, ferrocene with a small fraction of thiophene dissolved in ethanol, from the top of the furnace. They observed that CNT aerogels formed at the hot zone (1050 to 1200 °C) after injecting the catalyst-containing solution and then fluttered to the bottom of the furnace with flowing gases, followed by continuous collection in the forms of either mats or fibers depending on the post-treatment process. Figure 1E and F show a meter-wide CNT mat and a coil of CNT yarns synthesized by FCCVD, respectively. Mass production of CNT mats and yarns has been achieved and commercial products are available now (Nanocomp Technologies, Inc.). These mats are very promising for applications as strong composites, electro-magnetic interference (EMI) shielding, and current collectors in battery electrodes as discussed in Section 4.

Hydrocarbons such as n-hexane, methane, acetylene, and ethanol are readily pyrolysiszed at high temperature for efficient CNT growth. However, byproducts such as amorphous carbons and soot particles accumulate very fast on CNTs. Nikolaev et al. proposed to use carbon monoxide as carbon source, considering that the disproportionation of carbon monoxide only occurs in the presence of catalyst.[20] This indeed produced nanotubes with very clean surfaces. The problem of this method is the low nanotube yield, which forced to conduct the growth at high pressure with high safety risk. In addition, the as-produced SWCNT

**Jiangtao Di** received a PhD in physical chemistry from Suzhou Institute of Nanotech and Nanobionics, Chinese Academy of Sciences in 2013. Upon graduation he went to the Alan G. MacDiarmid Nanotech Institute of University of Texas at Dallas as a research associate. His research interests are the growth of nanocarbon materials (especially carbon nanotubes) and their applications in strong and multifunctional materials.

**Xin Wang** is currently a Postdoc Research Scholar in the Department of Materials Science and Engineering at North Carolina State University. She received her PhD in materials science and engineering from North Carolina State University in 2012. Her research expertise is in the fabrication and characterization of novel nanostructured and multifunctional CNT assemblies, high strength and lightweight nanocomposites, and mechanical, electrical, and thermal inter-relations at the nanoscale.

**Qingwen Li** received a PhD in chemistry from Tsinghua University in 2000. After 7 years research experience on carbon nanotubes at Peking University, Cambridge University, and Los Alamos National Laboratory, she joined Suzhou Institute of Nanotech and Nanobionics, Chinese Academy of Sciences, in 2007 as a professor of the "100 Talents Program" supported by the Chinese Academy of Sciences. Her current research interests focus on the synthesis and application of dry-processable carbon nanotubes.

**Yuntian Zhu** is a Distinguished Professor at North Carolina State University and Dean and Qianren Professor, Nanjing University of Science & Technology. He received a PhD Mater. Sci. Eng. at the University of Texas at Austin in 1994, a M.S. in Mater. Sci. Eng. at Oregon Graduate Inst. Sci. Tech. in 1991 and a B.S. in Metallurgy at Hefei University of Technology, China, 1983. Yuntian Zhu was the team leader of the Nanomaterials Team in MPA-STC, Los Alamos National Laboratory, before he joined the NCSU faculty in 2007. Zhu's research in recent years has focused on two major nano-related areas: metals and alloys with nano/ultrafine-grain structures, and the synthesis and processing of carbon nanotubes and CNT composites.

**Table 1.** Comparison of the dry-processing methods and solution-based methods for processing CNTs.

| Methods | Scalabillity | Dispersion | Purification | Time-consuming | Structure damage | Nanotube alignment |
|---|---|---|---|---|---|---|
| Dry-process method | Yes | No | CNTs by FCCVD: Yes; Spinnable arrays: No | No | No | Yes |
| Solution-based methods | Yes | Yes | Yes | Yes | Yes | No |

**Table 2.** Comparison of the properties of CNT films and composites prepared by dry-processing methods and solution-based methods.

| Types | Methods | Materials | Diameter [nm] | Density [g cm$^{-3}$] | Tensile strength [MPa] | Modulus [GPa] | Thermal conductivity [W m$^{-1}$ K$^{-1}$] | Electrical conductivity [S m$^{-1}$] | Ref. |
|---|---|---|---|---|---|---|---|---|---|
| CNT films | Solution-based methods | FWCNT | 3–8 | – | 80 | 14 | – | 14 940–29 400 | [11d] |
| | | SWCNT | – | – | 37 | 0.95 | – | 350 000 | [106] |
| | | SWCNT | 0.88–1.19 | 0.5 | 74 ± 2 | 5 ± 0.2 | | 12 000 | [11b] |
| | | SWCNT | – | 0.6 | 80 | 1.5 | – | – | [107] |
| | | SWCNT | 1.1–1.4 | 0.8 | 22 | 2 | – | – | [108] |
| | | SWCNT | – | – | 15 (as-prepared) | – | – | 15 000 (as-prepared) | [109] |
| | | | | | 60 (cross-linked) | | | 55 000 (cross-linked) | |
| | | MWCNT | – | – | 80 (random) | 1.04 (random) | – | 40 000 (random) | |
| | | | | | 100 (aligned) | 1.91(aligned) | | ∥: 60 000 (aligned) | |
| | | | | | 220 (aligned & cross-linked) | 8.8 (aligned & cross-linked) | | ∥: 620 000 (aligned &cross-linked) | |
| | | SWCNT | 1.0–3.0 | – | – | – | 2.24* | – | [110] |
| | | MWCNT | 30–100 | – | – | – | 1.68* | – | [111] |
| | | SWCNT | 1.3 | 0.6 | – | – | ∥: 60, ⊥: 11 | ∥: 29 411, ⊥: 4 743 | [112] |
| | | MWCNT | 40–60 | – | 7.5 | 0.785 | – | 10 000 | [113] |
| | | MWCNT | 10 | 1.39 | – | 2 | ∥: 766 ± 77 | ∥: 64 000 | [102] |
| | Dry-processing methods | MWCNT | 7–10 | 1.51 | 422.6 ± 17.4 | 10.1 ± 0.9 | – | – | [35d] |
| | | MWCNT | 15 | 0.62 | – | – | ∥: 153 | ∥: 20 000 | [97] |
| | | MWCNT | 30–50 | 0.84 ± 0.08 | 75.6 | – | ∥: 70 | ∥: 4 000 | [90d] |
| | | FWCNT | 5 | 0.9 | 1100–1900 | 90 | – | ∥: 35 000 | [11a] |
| | | FWCNT | 8 | 0.98 | 598 | 15.4 | – | – | [98] |
| Composites | Solution-based or melt-processing methods | MWCNT/PVA | 15 | – | 348 | 7 | – | – | [114] |
| | | MWCNT/PVA | – | – | – | 12.6 | – | – | [115] |
| | | MWCNT/PMMA | 20–50 | – | 80 | 3.7 | – | – | [116] |
| | | MWNT/PA-6 | <20 | – | 47 | 1.24 | – | – | [117] |
| | | SWCNT/PP | 1.3–1.5 | – | 36 | 1.19 | – | – | [118] |
| | | MWCNT/epoxy | 60–100 | – | – | – | 1.3* | – | [119] |
| | | MWCNT/PPS | 40–90 | 2.1 | – | – | 1* | $5 \times 10^{-12}$ | [120] |
| | | SWCNT/epoxy | <2 | – | – | – | 0.29* | 0.08 | [121] |
| | | SWCNT/PVA | – | – | 505 ± 67 | 15.6 ± 3.8 | – | – | [89c] |
| | | MWCNT/PA 6,6 | 50 | 2.1 | 625 | 56 | – | 41 700 | [93] |
| | Dry-process methods | MWCNT/epoxy | 8 | 1.5 | 402 | 22.3 | – | ∥: 7 700, ⊥: 4 200 | [90e] |
| | | MWCNT/epoxy | 20 | – | 231.5 | 20.4 | – | ∥: 10 000 | [90c] |
| | | MWCNT/BMI | 3–8 | – | 2088 | 169 | – | ∥: 550 000 | [90a] |
| | | MWCNT/BMI | 3–8 | – | 3081 | 350 | – | – | [90b] |
| | | MWCNT/PVA | 7–10 | 1.51 | 1600 ± 200 | 107 ± 16 | – | ∥: 78 000 | [122] |
| | | MWCNT/BMI | 7–10 | 1.51 | 3500 ± 420 | 266 ± 36 | ∥: 41 ± 2.5 | ∥: 123000 | [35b] |
| | | MWCNT/ polyimide | 7–10 | 1.51 | 227.7.0 ± 25.3 | 53.73 ± 3.29 | ∥: 18.4 ± 0.13 | ∥: 18300 | [123] |

Note: Values with "*" after them are thermal conductivities along the thickness direction. Others are the in plane thermal conductivities. For the films that are composed of aligned CNTs, the in-plane thermal conducitivity and electrical conductivity parallel (∥) to and perpendicular (⊥) to the nanotube alignment are given.

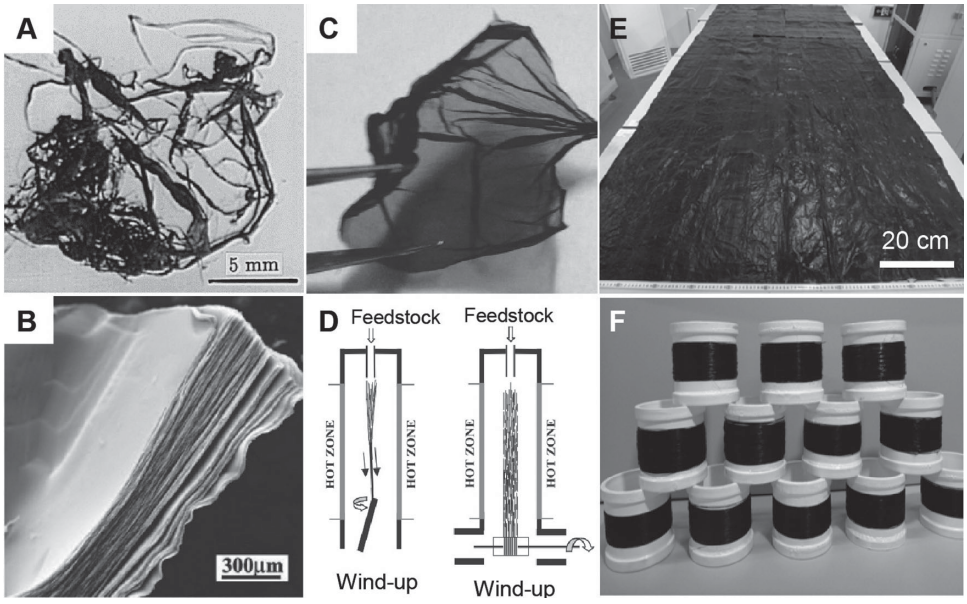


**Figure 1.** (A) Optical images of SWCNT ribbons synthesized by FCCVD. Reproduced with permission.[16b] Copyright 1998, Elsevier. (B) SEM image of a buckybook. (C) A freestanding single walled nanotube monosheet peeled from a buckybook with tweezers. Reproduced with permission.[18] Copyright 2009, American Chemical Society. (D) Schematic of continuous spinning (left) and collecting (right) process. Reproduced with permission.[14b] Copyright 2004, AAAS. (E) A large-area CNT film and (F) CNT threads prepared by FCCVD (Photographs courtesy of Suzhou Creative Nano-Carbon Co. Ltd.).

films or mats contained 75 wt% of ion impurity. In order to overcome this problem and improve the stability of nanotube growth, Nasibulin and co-workers introduced a small amount of $CO_2$ and $H_2O$ vapor into in the reactor and achieved continuous collection of large-area transparent and conducting CNT films at atmosphere pressure.[21] These additives were found to increase the length of nanotubes by etching amorphous carbon that can poison catalyst particles needed for CO disproportionation as well as for nanotube nucleation and growth. Moreover, the $CO_2$ could decrease the minimum temperature for nanotube synthesis from 890 °C to below 600 °C.[21] They showed that the CNT films after acid treatment could give a sheet resistance of 80 ohms per square (Ω/sq) at a transmittance of 90% at 550 nm, even superior to the typical performance of ITO coated on flexible polymer substrates.[21] We will further discuss the properties and applications of these transparent CNT films in section 3 and 4.

### 2.2. Vertically Aligned CNT Arrays

#### *2.2.1. Normal CNT Arrays*

Instead of floating catalysts in the gas stream, fixing catalysts on a substrate is one of the best approaches to grow high-purity CNT assemblies (arrays) directly. In a typical process for growing vertically aligned CNT arrays, catalysts are prepared by physical vapor deposition of a layer of catalyst film on a substrate such as Si wafer, and then annealing at high temperatures with diluted hydrogen atmosphere to form catalyst nanoparticles on the substrate. Hydrocarbon gases such as acetylene, ethylene or methane then catalytically decomposes on the catalyst particles to produce active carbon atoms, which diffuse to the step edges of the catalyst particles, reach saturation, and then precipitate out to form nanotubes.[22] Early works demonstrated that vertical CNT arrays could grow from the catalytic particles that are embedded in porous substrates such as silica and alumina.[23] In particular, Fan and co-workers reported the growth of highly-packed CNT arrays by CVD.[13b] They deposited a thin Fe film (5 nm thick) on a porous silicon substrate by electron beam evaporation and used it as catalyst. **Figure 2**A shows patterned CNT arrays grown at 700 ºC using ethylene as carbon source. The CNTs self-aligned perpendicularly to the silicon substrate because of the high packing density of nanotubes and strong inter-tube interactions (e.g. van der Waals forces).[13b]

Hata et al. developed an efficient method (well known as the "super-growth") for growing SWCNT arrays.[13c] They were able to grow a 2.5-mm high SWCNT array in ten minutes by introducing a trace amount of water vapor to the growth atmosphere (Figure 2B and C). The water vapor acted as a weak oxidizer to etch the amorphous carbon coated on the catalyst particles, which considerably prolonged the activity of the catalyst. It could also inhibit the aggregation of catalyst particles on the substrates.[24] Further study revealed that a series of oxygen-containing molecules are capable to enhance nanotube growth when combined with a carbon source that does not contain oxygen.[25] In addition to the growth enhancers, Hata et al. added an alumina buffer layer between the silicon substrate and the catalyst film (iron film, deposited by electron beam evaporation),[13c] which helped sustain the activity of the catalyst by inhibiting the diffusion of the catalyst into the substrate.[26] Both the growth enhancer and efficient buffer layer promote the growth of CNT arrays with long length and at high rate. By further optimizing the growth condition, CNT arrays in

  

NANO MICRO small

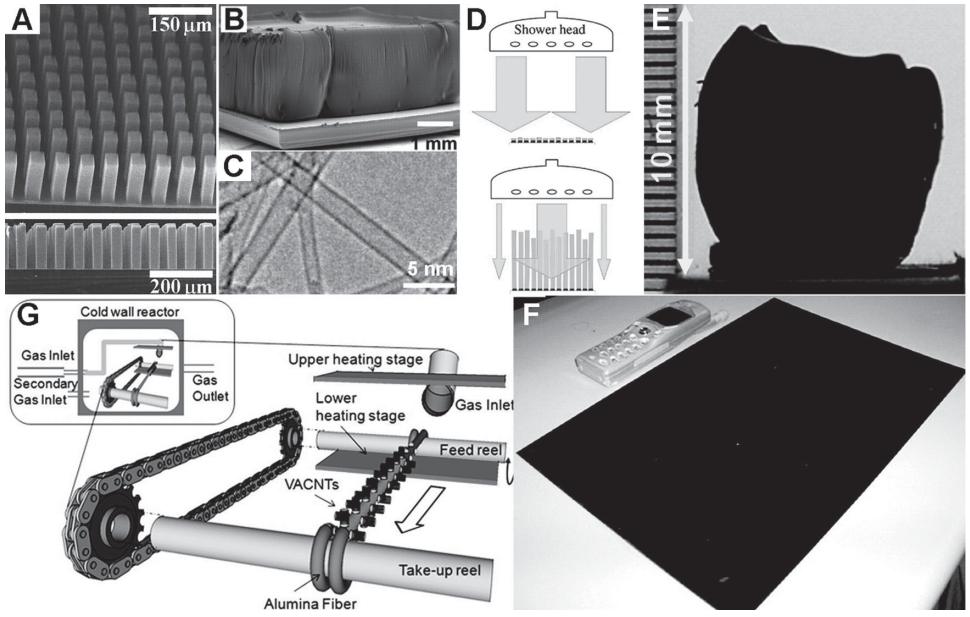


**Figure 2.** (A) SEM image of patterned CNT arrays. Reproduced with permission.[13b] Copyright 1999, AAAS. (B) SEM image of a 2.5-mm-tall SWCNT array and (C) TEM image of the nanotubes. Reproduced with permission.[13c] Copyright 2004, AAAS. (D) Schematic of a shower growth system showing gases delivered from the top of the CNT array. (E) A centimeter-long CNT array. (F) Photograph of a CNT array grown on an A4-size substrate. Reproduced with permission.[27b] Copyright 2009, American Chemical Society. (G) Cold-wall reactor system developed for continuous growth of vertically aligned nanotube arrays. Reproduced with permission.[29] Copyright 2011, American Chemical Society.

centimeter-long and in large area have been achieved.[27] For example, Hata's group introduced a shower system in which gases including water vapor were delivered evenly to catalysts from the top of CNT arrays (Figure 2D). Figure 2E and Figure F show a centimeter-long CNT array and a CNT array grown on in A4 size substrate, respectively.[27b] Recently, Villoria demonstrated continuous production of vertically aligned CNT arrays (Figure 2G).[27b,28] Catalyst ($Fe/Al_2O_3$) substrates were placed on a movable quartz stage between a bottom heater and a top heater in their smartly designed growth system. They were able to grow millimeter tall-aligned MWCNT arrays at a moving speed of 2.4 mm/s. Moreover, the method was suitable to grow aligned CNTs on 2D and 3D substrates.[29]

### *2.2.2. Spinnable CNT Arrays*

A unique type of CNT arrays, known as spinnable arrays, has attracted considerable interest in recent years. They can be continuously transformed from the vertically aligned state into a horizontally aligned CNT film by a simple dry drawing method.[9] Jiang and co-workers reported the first spinnable CNT array in 2002.[9a] They found that picking a small nanotube bundle off the edge of an array led to the formation of a continuous CNT thread. They also showed that only the CNT arrays that had good alignment were spinnable.[30] Zhang et al. demonstrated that twisting a nanotube film during the drawing process gave a strong and flexible CNT fiber.[31] They further showed a 5-centimeter-wide, meter-long transparent CNT film drawn from a spinnable array at a rate of ~7 m per minute as shown in **Figure 3**A.[9b] The films are flexible, free-standing, transparent, conductive, and have nanotubes well aligned, which have enabled various applications as discussed in section 3 and 4. By optimizing the growth conditions, Jiang and coworkers were able to continuously draw a high quality nanotube sheet from a nanotube array on an 8-inch wafer as shown in Figure 3B.[10]

The growth approaches for spinnable CNT arrays are very similar to those for normal arrays. The critical issue for growing spinnable arrays is to prepare catalysts that have proper areal distribution density of particles and uniform particle sizes. Two widely used catalyst layer structures are $Fe/SiO_2/Si$ and $Fe/Al_2O_3/SiO_2/Si$. Both of them are commonly prepared by depositing nanometer-thin target layers on a silicon wafer with a layer of $SiO_2$ using physical vapor deposition (e.g. electron beam evaporation). The $Fe/SiO_2/Si$ catalysts usually come with acetylene as the carbon source and they give MWCNTs (3–12 graphitic walls, and ~10 nm in diameter).[31,32] The $Fe/Al_2O_3/SiO_2/Si$ catalysts produce few-walled CNTs (2–4 graphitic walls, and ~5 nm in diameter) when ethylene is used as the carbon source.[11a,33] The $Al_2O_3$ layer helps with the formation of uniformly distributed nano-size catalyst particles by restricting particles from aggregation and diffusion. Recently, we achieved spinnable double-walled CNT arrays (>90% nanotubes are double-walled) by optimizing the growth conditions (Figure 3D).[33] Figure 3C shows our spinnable double-walled CNT arrays grown on 4-inch silicon wafers using batch growth in automatic 7-inch CVD furnace. Iron (II) chloride was also used as catalyst for growing spinnable CNT arrays. It usually catalyzes the growth of large-diameter MWCNTs (>20 graphitic walls, and 20–50 nm in diameter).[34] Our previous study demonstrated that the fibers, films and composites prepared using small-diameter CNTs have much better mechanical performance than large-diameter MWCNTs.[11a,35] Because the growth of CNT arrays is dominated by a base-growth

  

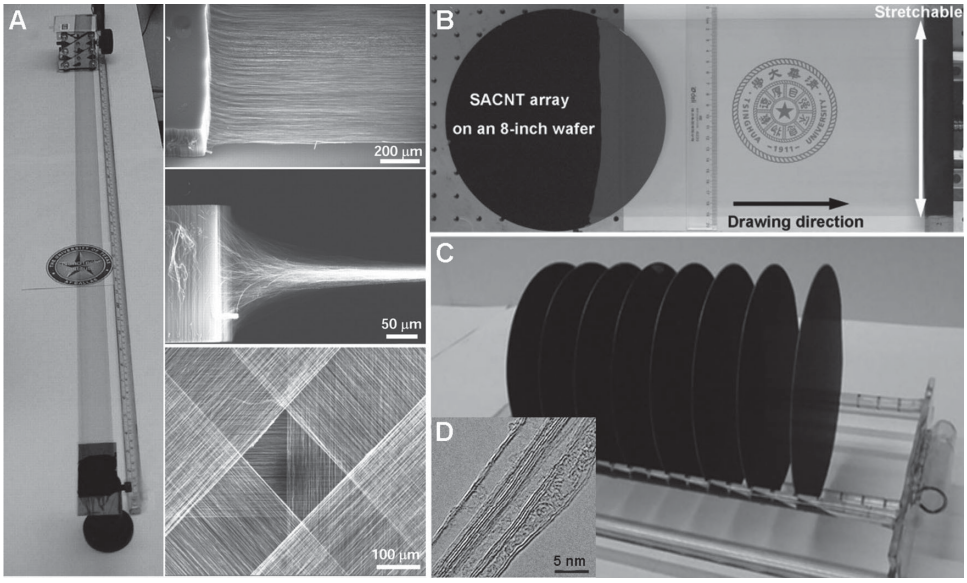


**Figure 3.** Spinnable CNT arrays. (A) A meter-long CNT film drawn from spinnable array and their SEM images. Reproduced with permission.[9b] Copyright 2005, AAAS. (B) Photograph showing a transparent CNT film drawn from an 8-inch wafer. (C) Batch growth of 4-inch spinnable CNT wafers. (D) TEM image of double-walled CNTs in a spinnable array. Reproduced with permission.[33] Copyright 2013, Wiley-VCH Verlag GmbH & Co. KGaA.

mode,[36] and most of the catalyst particles remained on the substrate after the removal of CNTs.[32d] This means the CNT films drawn from spinnable arrays are of high purity.

The drawing mechanism of spinnable nanotube arrays has been controversial for years due to the complexity of the drawing processes. Descriptively, CNTs were drawn from their arrays typically in the form of small bundles that contain about 50-100 nanotubes. Zhang et al. proposed that the continuity of CNT films is maintained by initiating new nanotube bundles at the top and bottom of spinnable arrays.[32a] This means that the interaction force varies along the nanotube array. Indeed, Gilvaei et al. reported that the drawing force at the top of a CNT array was several times higher than that in the middle of the array.[37] Zhu et al. attributed the continuity of the drawing process to the formation of entangled structures when the pulling process approached the ends of an spinnable array.[38] Kuznetsov et al. developed a self-strengthening spinning model,[39] with the following key components: 1) a network of individual nanotubes or small bundles interconnecting with larger bundles in a spinnable array, 2) preferentially peeling off the interconnecting bundles, and 3) self-strengthening of these interconnections by densification at the top and bottom of the nanotube array during drawing. By comparing the morphologies of the normal and spinnable CNT arrays, Zhang and co-workers proposed that the well-aligned CNT arrays have good spinnability. However, nanotube alignment alone cannot be used as judge if an array is spinnable or not. For example, SWCNT arrays are not spinnable although the nanotubes have very good alignment.[40] Our experimental results indicate that both good alignment and appropriate volumetric density are required for a CNT array to be spinnable.[32d] Their optimum combination gives proper heterogeneity of tube–tube interactions that facilitate spinning. Experimental study showed that the well-aligned CNT arrays composed of 10-nm-thick nanotubes were spinnable when the number density of CNTs was between $3–10 \times 10^{10}$ $cm^{-2}$.[32d]

## 3. Applications for Functional Thin-Film Devices

Thin CNT films are flexible, transparent and conductive. They have the potential to serve as transparent electrodes to replace the resource-limited and brittle indium tin oxide (ITO) transparent electrodes for the next generation optoelectronic devices.[41] They are also promising to act as conducting scaffolds with large surface area for semiconductors to prepare functional devices. In this section, we will first discuss the advantages of dry-processable CNTs in terms of making transparent electrodes and their performance and then discuss the functional film devices that are fabricated using dry-processable CNTs.

### 3.1. Transparent CNT Films

Solution-based methods, such as vacuum filtration,[42] solution spray,[43] and dip coating,[44] have been developed to prepare thin CNT films with high transparency and low sheet resistance.[41b] In comparison, CNT films that are prepared from dry-processable CNTs show comparable performance, but are much more straightforward to prepare. As mentioned in section 2, transparent CNT films can be collected downstream of a furnace reactor or drawn from spinnable arrays (**Figure 4**). The dry state processing eliminates the complex processes in the solution-based methods such as purification, surfactant-assisted ultrasonic dispersion, film deposition, and film exfoliation.[45] It avoids structural damages of CNTs that usually occurs in solution-based methods. In addition, the

  

NANO MICRO small

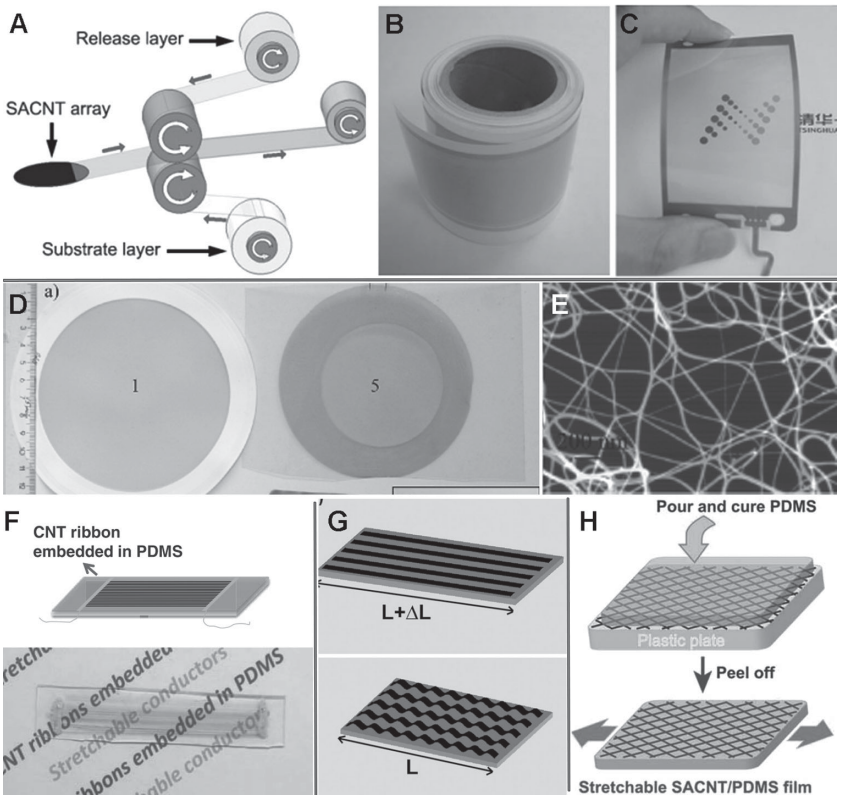


**Figure 4.** (A) Schematic showing the roll-to-roll process for producing nanotube films and (B) the produced CNT films. (C) Nanotube film based touch screen. Reproduced with permission.[49] Copyright 2011, Wiley-VCH Verlag GmbH & Co. KGaA. (D) Photograph of nitrocellulose filters with collected single walled nanotube films and (E) SEM image of the nanotube films. Reproduced with permission.[21] Copyright 2011, American Chemical Society. (F) An aligned CNT film embedded in PDMS for stretchable conductor. Reproduced with permission.[50] Copyright 2010, Wiley-VCH Verlag GmbH & Co. KGaA. (G) A prestrain-release method for preparing buckled stretchable CNT/PDMS composite conductors. Reproduced with permission.[51] Copyright 2012, Wiley-VCH Verlag GmbH & Co. KGaA. (H) Fabrication and properties of cross-stacked (45°, 45°) CNT/PDMS film. Reproduced with permission.[52] Copyright 2012, Wiley-VCH Verlag GmbH & Co. KGaA.

freestanding feature of dry-processed films makes it easy to transfer them, whereas the transfer of the vacuum-filtrated CNT films is still a challenge.

Transparency and conductivity are two key indexes for transparent electrodes. They correlate with each other by $T=\left(1+\frac{Z_0}{2R_s}\frac{\sigma_{op}}{\sigma_{dc}}\right)^{-2}$, where $T$ is the transmittance, $R_s$ is the sheet resistance, $Z_0$ (376.73 Ω) is the characteristic impedance of vacuum, and $\sigma_{dc}$ and $\sigma_{op}$ are the DC and optical conductivity, respectively.[46] The ratio of $\sigma_{dc}/\sigma_{op}$ is the figure of merit (FOM). A high $\sigma_{dc}/\sigma_{op}$ value indicates a thin film with high conductivity and low optical absorption. CNT films prepared by the dry-processable methods typically have $\sigma_{dc}/\sigma_{op}$ lower than 5,[9b,30,47] which is consistent with dopant-free nanotube films prepared by other methods.[43,48] However, they cannot meet the minimum requirement of 16 for flat panel displays, which means a sheet resistance of ~100 Ω/sq and transparency of 80% at 550 nm. Strategies such as doping or metal coating have been developed to improve the conductivity of CNT films. Kaskela et al. reported that SWCNT films prepared by FCCVD had a sheet resistance of as low as 110 Ω/sq at 90% optical transmittance (at 550 nm) after being doped by acid.[47a] The corresponding $\sigma_{dc}/\sigma_{op}$ was ~32. Feng et al. reported roll-to-roll preparation of CNT thin films using spinnable arrays as shown in Figure 4A.[49] Highly conductive and transparent nanotube films (208 Ω/sq, 90% and 24 Ω/sq, 83.4%) was achieved after suitable laser trimming and deposition of metals on the films,[49] which produced a $\sigma_{dc}/\sigma_{op}$ value as high as ~82. They further demonstrated the fabrication of touch screens using the CNT films from spinnable arrays as shown in Figure 4B–C.[49] Benefiting from the unique properties of CNTs, the nanotube-based touch screens are flexible, durable, energy saving and resistant to water, humidity and EMI.[49] Smart cell phones and other display products that use CNT films as transparent electrodes are commercially available (CNTouch).

CNT films are suitable for preparing robust and stretchable conductors. Zhang et al. reported a transparent and stretchable film conductor by embedding an aligned CNT film in poly(dimethylsiloxane) (PDMS) (Figure 4H).[50] The CNT/PDMS film showed a large increase in electrical resistance when stretched to 100% strain at the first time because of the decreased contact area between nanotubes. After the first stretch-release cycle, the resistance of the film became very stable even after 30 cycles. Xu et al. transferred an aligned CNT film onto a pre-strained PDMS film and released the CNT/PDMS film to form a buckled structure as shown in Figure 4G.[51] The buckled CNT/PDMS film showed a very small increase of 4.1% in resistance when stretched to the pre-strain of 100%. The aligned CNT films are anisotropic in electrical conductivity. The sheet resistance perpendicular to the nanotubes is 50–70 times higher than that parallel to the nanotubes.[9b] Liu and coworkers reported the preparation of cross-stacked aligned CNT films for transparent and stretchable conductors (Figure 4H).[52] The cross-stacked CNT films showed isotropic resistance but anisotropic mechanical properties. By embedding the cross-stacked CNT films in a PDMS film, the composite film showed nearly unchanged resistance after 200 stretch-release cycles with a maximum strain of 15%.[52]

### 3.2. Solar Energy Harvesting Devices

For solar energy applications, films from dry processable nanotubes have been applied as either transparent electrodes or catalytic electrode in several types of solar energy harvesting devices such as nanotube-silicon solar cells, photoelectrochemical cells, and organic photovoltaic cells.

  

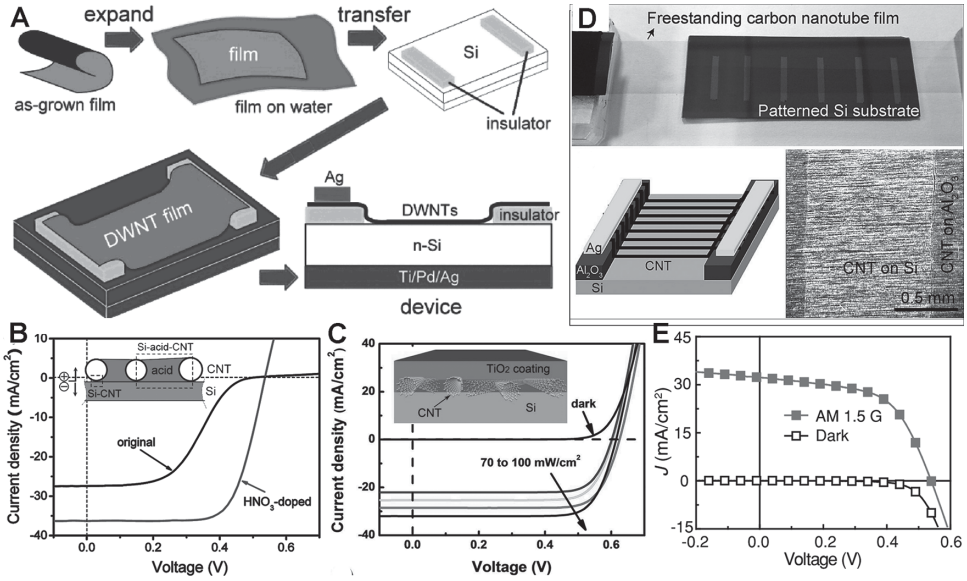


**Figure 5.** (A) Illustration of the fabrication process of nanotube/n-Si solar cell. The as-grown nanotube films fully expanded in a water solution and then were transferred to a patterned Si substrate. Reproduced with permission.[53] Copyright 2007 American Chemical Society. (B) *J–V* characteristics of the solar cell before (black curve) and after (red) infiltration of dilute $HNO_3$. Conversion efficiency increased from 6.3% to 13.8% after acid infiltration. Reproduced with permission.[57] Copyright 2011 American Chemical Society. (C) *J–V* curves of a $TiO_2$-nanotube-Si solar cell measured in the dark and light conditions (from 70 to 100 mW/cm$^2$). The efficiency was 15.1% at 100 mW/cm$^2$. Reproduced with permission.[60] Copyright 2012 Nature Publishing Group. (D) Preparation of the Si hybrid solar cells using aligned carbon nanotube drawn from spinnable nanotube arrays and the structure and optical image of the device. (E) *J–V* characteristics of an aligned nanotube–Si solar cell under one sun (AM 1.5 G) illumination and dark). Reproduced with permission.[33] Copyright 2013 Wiley-VCH Verlag GmbH & Co. KGaA.

Wei et al. reported the utilization of a double-walled CNT film prepared by floating catalyst CVD as a transparent electrode for silicon hybrid solar cells.[53] The device was achieved by simply transferring a nanotube film to a patterned silicon substrate as shown in **Figure 5**A. Its power conversion efficiency was as high as 7.4%.[54] The CNT films in such devices function as both transparent charge collecting electrodes and a counterpart for the formation of heterojunction (Schottky junction[55] or p-n junction[56]. By doping the nanotubes with strong acids such as $HNO_3$, Jia et al. further improved the conversion efficiency up to 13.8% as shown in Figure 5B.[57] The acid improves the conductivity of the nanotubes by p-type doping,[58] and also helps the formation of a thin layer of oxide to prohibit the charge recombination.[59] Recently, Shi and co-workers reported a high conversion efficiency of ~15% for the silicon hybrid solar cells, which is comparable to that of commercial silicon solar cells as shown in Figure 5C.[60] In their approach, they applied a layer of titanium oxide particles on the device to reduce the light reflection, and meanwhile doped the CNT film with $HNO_3$. As mentioned in Section 2.1, the CNT films prepared by FCCVD methods contain many types of impurities such as amorphous carbon and metal catalyst particles. It is desirable to remove them prior to device fabrication in order to eliminate their influence on the device performance. CNT films drawn from spinnable arrays are of high purity as shown in Section 2.2. We recently demonstrated their application in fabricating CNT-silicon hybrid solar cells as shown in Figure 5D.[33] The device fabrication processes were simplified considerably due to the fast and easy dry drawing process and the exemption of the purification of nanotubes. Although the films were not as conductive as the films from floating catalyst CVD process as mentioned in Section 3.1, the conversion efficiency of the devices reached up to 10.5% as shown in Figure 5E,[33] which was even higher than that of the devices fabricated using pristine nanotube films prepared by floating catalyst CVD.[47c,54,61] We attributed it to the good alignment of the nanotubes in the spinnable array-based films, which could form high nanotube-silicon junction. Indeed, a device using aligned nanotubes showed a 3.2-imes higher efficiency than that with random nanotubes that were prepared from the same nanotube array.[33]

Photoelectrochemical cells include dye- or quantum dot-sensitized solar cells and solar water splitting cells. A typical photoelectrochemical cell is composed of an anode, a cathode, and electrolyte.[62] For an n-type anode, the anode absorbs light and converts it to electricity (dye-sensitized solar cells, DSSC) or hydrogen (water-splitting cells). Dry-processable CNT films have been applied as a catalyst component of cathodes in dye-sensitized solar cells with the aim of replacing the high cost and scarce platinized cathodes. It was recently reported that the charge transfer resistance of the CNT-catalyzed cathodes was several times lower than that of the Pt-catalyzed cathodes in the disulfide/thiolate[63] and Co(II/III)tris(2,2′-bipyridyl)[64] redox mediators. As for commonly used $I^-/I_3^-$ electrolyte, CNTs showed comparable charge transfer resistance with Pt.[63] Conversion efficiency of solar cells using nanotube-catalyzed cathodes in disulfide/thiolate electrolyte was 5.81%, higher than 4.54% for the solar cells using Pt-catalyzed cathodes.[63] Comparable efficiency was also achieved in Co(II/III)tris(2,2′-bipyridyl) and $I^-/I_3^-$ redox electrolyte.[63,65] Yang et al. reported the usage of

  

NANO MICRO small

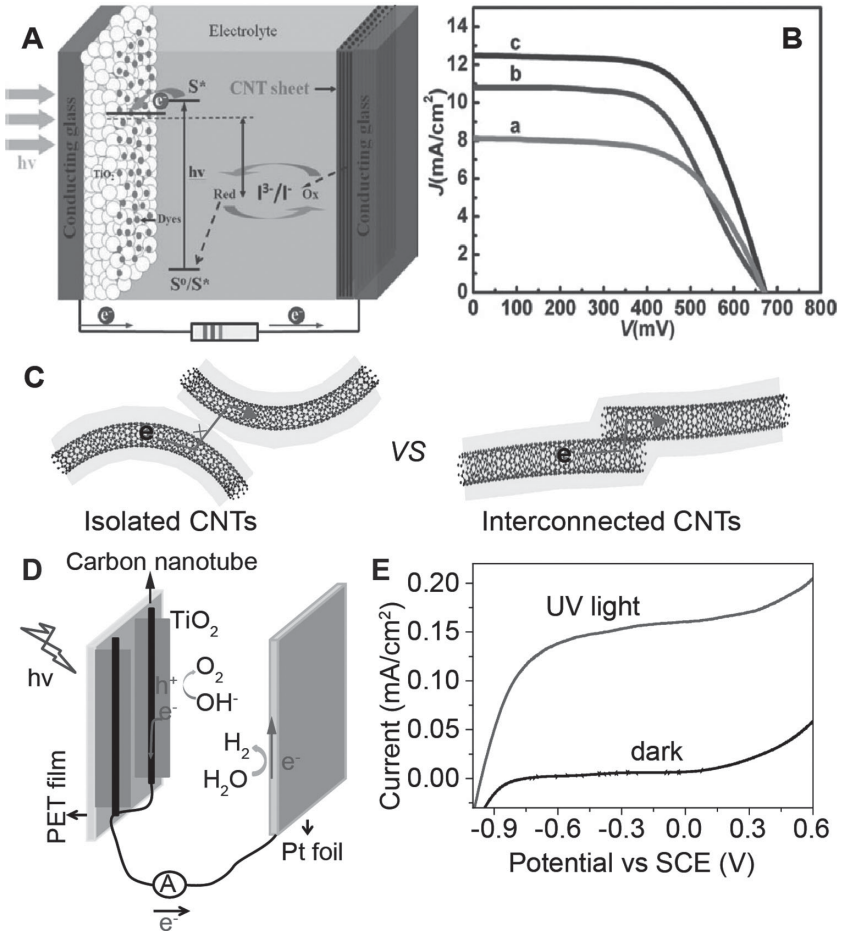


**Figure 6.** (A) Schematic illustration of a novel dye-sensitized solar cell using a CNT sheet as the counter electrode. (B) Current–voltage characteristics of the typical dye-sensitized solar cells by using the randomly dispersed pristine CNT film (a), the aligned multi-walled CNT sheet (b), and the platinum (c) as counter electrodes. The curves were obtained under AM 1.5 illumination. Reproduced with permission.[65] Copyright 2011 WILEY-VCH Verlag GmbH & Co. KGaA. (C) Schematic illustrating that charges transfer more smoothly between nanotubes that are interconnected inside of oxide coatings (right) than those isolated by oxide coatings (left). (D) Schematic illustrating the structure of a water-splitting solar cell containing a nanotube/$TiO_2$ film in which nanotubes serve as the charge transport paths and current collector. (E) Current–potential curves of a nanotube/$TiO_2$ film under dark and UV illumination. Reproduced with permission.[66] Copyright 2012 WILEY-VCH Verlag GmbH & Co. KGaA.

aligned CNT films as the catalytic component in the counter electrode of a DSSC as shown in **Figure 6**A.[65] Their results showed that the energy conversion efficiency of the resulting cell was higher than that of devices using randomly dispersed carbon nanotube films and comparable with that of devices using the platinum (Figure 6B). We reported a novel anode for water splitting cells, in which continuous $TiO_2$ was coated on a freestanding CNT film.[66] The nanotubes were well-aligned and interconnected inside of the conformal oxide coating, achieving efficient conducting paths, which sharply contrasted to that of the nanotube/$TiO_2$ hybrids synthesized by the wet chemistry approaches as shown in Figure 6C. The nanotube films acted as scaffold, charge transport path, and charge collecting electrode simultaneously. Upon light illumination, photogenerated and separated electrons in $TiO_2$ transport through nanotubes to the external circuit as shown in Figure 6 (D and E). Moreover, the hybrid film is robust, and can generate stable photocurrent even after being bent for hundreds of times.[66]

### 3.3. Supercapacitors and Batteries

Dry processable CNT films can act as charge collectors and high surface area scaffolds for active materials of supercapacitors and lithium ion batteries. Firstly, as mentioned in section 3.1, conducting paths are formed in dry processable nanotube films via interconnected nanotubes. When compounded with active materials, the interconnected structure can transport charges very efficiently, and even make devices free from traditional metal charge collectors such as aluminum and copper foils. In comparison, for nanotube-incorporated active composites prepared by solution-based method,[67] the potential of nanotubes in conductivity enhancement has not been fully utilized due to the isolation of nanotubes by active materials, and charge collectors are still required. Secondly, dry processable nanotube films can adjust their porous structures to adapt to the volume change of active materials during electrochemical processes, which avoids the problem of detachment of active materials for metal foil charge collectors. Thirdly, the large surface area of dry processable nanotubes promises strong adhesion of active materials on nanotubes, making it unnecessary to use binders in the nanotube composite electrodes. Lastly, dry processable CNT films is strong, flexible, transparent, and lightweight (e.g. 1.5 mg/cm$^3$ for nanotube films from spinnable arrays[9b] and thus are promising for making portable, flexible and lightweight energy storage devices. Based on these advantages, high performance energy storage devices have been reported using various active materials such as poly(3,4-ethylene-dioxythiophene),[68] polyaniline,[69] $MnO_x$,[70] NiO,[70a] $Co_3O_4$[70a] for supercapacitors and $Fe_3O_4$,[71] graphite,[72] silicon,[73] $SnO_2$[74] for lithium ion batteries, respectively.

In the following section, we will present a few examples to demonstrate the superiority of dry processable CNT films as charge collecting electrodes for supercapacitors and lithium ion batteries. Kim and co-workers electrodeposited $MnO_x$ active layers onto aligned nanotube films drawn from spinnable nanotube arrays and characterized the electrochemical capacitance of the composite film using the aligned nanotubes as charge collector (**Figure 7**A).[70b] The oxide coated the surfaces of nanotubes in a conformal way as shown in Figure 7B. High specific capacitances of ~1250 F/g (Figure 7C, right) and excellent cycling stability (Figure 7C,

  

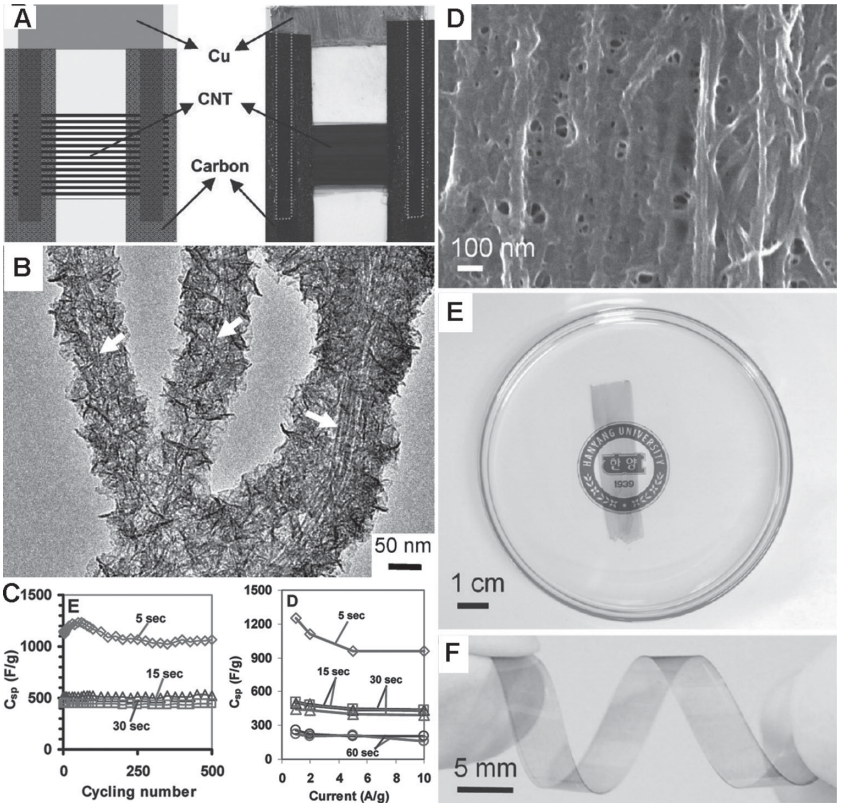


**Figure 7.** (A) A schematic representation and image of a nanotube film electrode. (B) A TEM image of a nanotube/$MnO_x$ composite film. (C) Cycling performance (left) and specific capacitance (right) of composite films deposition and for different time. Reproduced with permission.[70b] Copyright 2011 American Chemical Society. (D) SEM image showing the morphology of a hybrid nanomembrane. Photographs of a freestanding and optically transparent hybrid nanomembrane in ethanol (E) and a helically twisted hybrid nanomembrane/PET film (F). Reproduced with permission.[68] Copyright 2011 American Chemical Society.

left) were achieved by tuning the deposition time. By coating conductive polymers on aligned nanotubes, Lin[75] and Lee[68] independently developed transparent and flexible supercapacitors as shown in Figure 7D–F. Yu et al. developed stretchable supercapacitors by applying buckles on single walled nanotube films.[76] Wang and co-workers compared nanotube films with commonly used copper foils as charge collectors for lithium ion batteries,[72] and found that nanotube films had much stronger adhesion with graphite than copper foils (**Figure 8**A and B). The cycling and rate performance of the lithium ion batteries using nanotube films as charge- collecting electrodes is superior to the that of the batteries using copper foils as shown in Figure 8C.[72]

Fu et al. recently reported an aligned CNT–silicon film as a novel structure for flexible lithium ion battery electrodes.[73] Silicon layers were coated around nanotubes in aligned films by a CVD method using silane as the silicon source. In order to enhance the conductivity of composite films, an additional layer of carbon was coated on the nanotube–silicon core–shell composites, forming a nanotube–silicon–carbon hybrid structure as shown in Figure 8D. The hybrid showed high columbic efficiency of 94% after 45 cycles at a current density of 100 mA/g, with a resultant charge capacity of 1494 mAh/g (Figure 8E, left). Moreover, the hybrid also showed good rate capability as shown by the right panel in Figure 8E. A spring-like deformation behavior was observed in the nanotube–silicon–carbon hybrids during the lithiation/delithiation process, which possibly stabilized the cycling performance of the lithium ion batteries.

### 3.4. Other Applications of Dry-Processable CNTs

The unique structures of the dry processable CNT films have also made some other advanced energy conversion devices a reality. For example, Aliev et al. reported that CNT films drawn from spinnable arrays expanded 220% in width upon applying high-voltage static electricity as shown in **Figure 9**A.[77] Strong electrostatic repulsion between nanotubes occurred and led to the film expansion when static voltage is applied. The expansion disappeared very fast after the removal of voltage due to the good electrical conductivity of the nanotubes. Nanotube film-based actuators can serve at extreme temperature (80–1900 K) with giant strokes and strain rates.[77] Moreover, the actuation mechanism provides an effective approach to tune the density of nanotube films for other device optimization. As shown in Figure 9B, Fan's group developed a novel loudspeaker using the aligned nanotube films drawn from spinnable nanotube arrays (see Figure 9B).[78] They found that the nanotube films could generate audial sound when fed by audio frequency electric currents, due to the thermoacoustic effect. The nanotube loudspeaker showed a wide frequency response range of $10^2$–$10^4$ kHz, benefiting from the small heat capacity per unit area of nanotube thin films (estimated as $7.7 \times 10^{-3}$ J/m$^2$ K for a single nanotube film, 260 times lower than a 0.7 μm thick Pt film). Compared with traditional loudspeakers, the CNT-based loudspeakers are magnet-free, flexible, stretchable, and even transparent (Figure 9B). They can be freestanding or attached onto any insulating substrates (Figure 9B). Aliev and co-workers further extended the application of the nanotube thermoacoustic loudspeaker from air to water (Figure 9C).[79] A wide response range of 1–$10^5$ HZ was achieved.[79] Wei et al. recently demonstrated thermoacoustic chips fabricated by aligning CNT yarn arrays across grooves on silicon substrates as shown in Figure 9D.[80] The nanotube yarn arrays were achieved by tailoring aligned nanotube film from spinnable arrays by laser. This is a big step for the nanotube thermoacoustic loudspeakers toward commercialization. Other important applications of the dry processable CNT thin films include TEM grids,[81] incandescent display,[82] transparent electrodes in organic light-emitting diodes,[83] and scaffolds for surface-enhanced Raman scattering,[84] planar-defect-rich ZnO nanoparticles

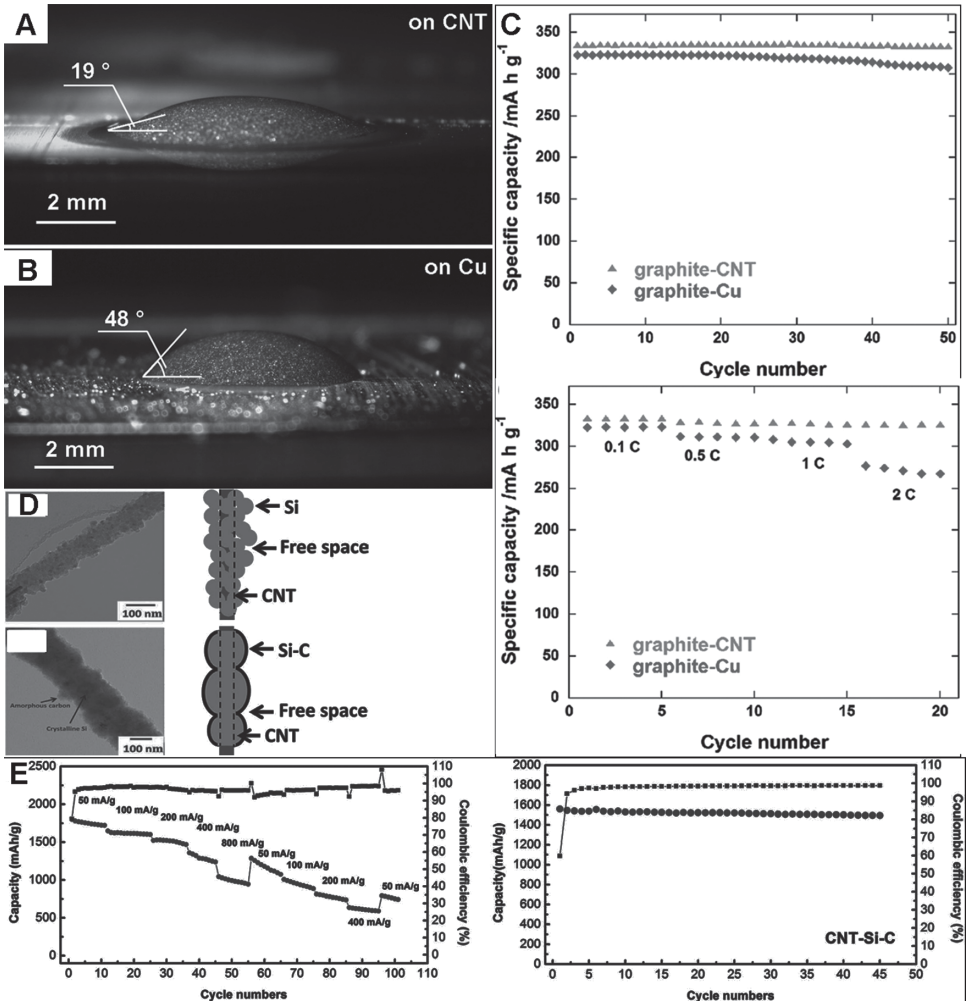


**Figure 8.** Photographs of graphite slurry droplets on: (A) a porous CNT film and (B) a flat Cu foil. The smaller contact angle and the larger droplet diameter on the CNT film reveal better wetting and easier slurry infiltration at the graphite/CNT interface than at the graphite/Cu interface. (C) Cycling (0.1 C, top) and rate performances (bottom) of the graphite-nanotube and graphite-Cu electrodes, revealing the superior electrochemical properties of the graphite-nanotube electrodes. Reproduced with permissionfrom.[72] Copyright 2013, WILEY-VCH Verlag GmbH & Co. KGaA. (D) Structures of nanotube–silicon and nanotube–silicon–carbon hybrids. (E) Cycle performance at 100 mA/g (left) and rate capability cycled at different current densities (right) in the potential window of 0.01–1.0 V. Reproduced with permission.[73] Copyright 2013, WILEY-VCH Verlag GmbH & Co. KGaA.

as ultraviolet emitters and photocatalysts,[85] and 3D copper nanostructures for $CO_2$ reduction.[86]

## 4. Novel Strategies for High-Performance and Multifunctional Composite Films

Preparation of engineering materials with high strength, high electrical and thermal conductivities is another hot area where CNTs play a very important role. Because CNTs have highly anisotropic properties, they need to be aligned in preferred orientation in order to obtain the best mechanical or physical properties. The CNT films prepared by solution-based methods are composed of random and short nanotubes. Their tensile strengths are usually below 100 MPa, and similarly their composites show poor mechanical performance. Approaches such as magnetic or electric field,[87] and shear flow,[88] have been used to align CNTs in polymer matrix. However, these approaches have some challenges, including difficult CNT dispersion, entanglement of long nanotubes, and low CNT volume factions. Due to these challenges, CNT/polymer structural composites synthesized by the wet dispersion method usually have low strengths (≤600 MPa).[89]

The nanotube alignment in dry processable CNTs can be improved by post drawing processing. For the CNT films prepared by FCCVD, simple stretching of the films can significantly improve nanotube alignment. For the CNT films drawn from spinnable arrays, most of the CNTs are well aligned along the drawing direction. The length-to-diameter ratio of dry processable CNTs is in the range of $10^3$ and $10^5$, much higher than that of the CNTs processed by wet chemistry. These unique features help utilize the unique properties of CNTs to prepare novel CNT films and composites.[35b,35d,90] Table 2 compares the properties of CNT films and composites prepared by solution-based methods and dry-state methods in terms of tensile strength, Young's

  

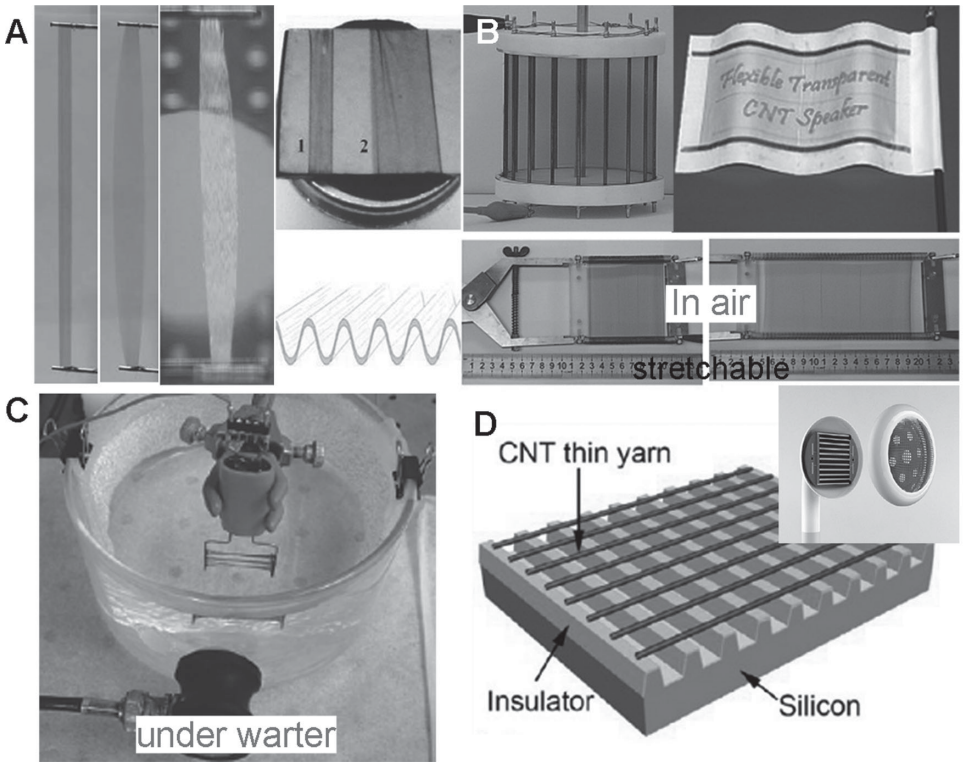


**Figure 9.** (A) CNT film actuators driven by high static voltage. Reproduced with permission.[77] Copyright 2009, AAAS. (B) CNT thermoacoustic loudspeakers in air. Reproduced with permission.[78] Copyright 2013 American Chemical Society. (C) CNT thermoacoustic loudspeakers under water. Reproduced with permission.[79] Copyright 2010, American Chemical Society. (D) A sketch of nanotube yarn array based thermoacoustic chip and the exploded view of a thermoacoustic earphone. Reproduced with permission.[80] Copyright 2013, American Chemical Society.

modulus, and electrical and thermal conductivities. Usually, the dry processable CNTs sheets are directly incorporated into polymer matrix (thermoplastic or thermosetting) without the need for dispersion. Currently, the architectures of the composites comprising of dry processable CNTs fall into three types. Type I, aligned CNT arrays are directly used as nano-fillers in continuous polymer matrix. The aligned CNT arrays play the role of free-standing continuous reinforcements in polymer,[91] or be shear-pressed into aligned sheet before polymer infiltration.[90e] Composites assembled from shear-pressed CNT arrays showed a tensile strength of ~400 MPa. Type II, CNT films are mechanically stretched to induce CNT alignment and subsequently infiltrated with polymer matrix.[90a,90b] CNTs were assembled into buckypapers in which CNTs are highly aligned to enable tensile strength to up to 3.1 GPa, elastic modulus of 350 GPa and electrical conductivity of ~$5 \times 10^3$ S/cm.[90b] Type III, aligned CNTs drawn from spinnable arrays were infiltrated with polymer by spin-coating or casting,[92] resin transfer molding,[49] or spraying–winding.[35b]-d Nanotube alignment can be improved by stretching CNTs before[35b] or after[93] incorporation of polymers. We have prepared ultrastrong aligned CNT composites that are 3.8 GPa in tensile strength, 293 GPa in Young's modulus, and (293 GPa), and 41 W $m^{-1}$ $K^{-1}$ in thermal conductivity.[35b] The opportunities for applications emanating from the remarkable mechanical and physical properties of aligned CNT/polymer composites are extraordinary, including structural and multifunctional components for aerospace vehicles, automotive structures, electromagnetic interference shielding, and thermal management.

### 4.1. Processing Aligned MWCNT Arrays into Flexible and Conductive Composites

Freestanding arrays of millimeter-long MWCNTs have unique compressive properties,[35d,94] fatigue resistance and viscoelastic characteristics.[95] They can be incorporated into polymer matrices, such as polydimethylsiloxane (PDMS),[95] and epoxy,[91b,96] for high-performance composites. For example, the MWCNT/PDMS composites exhibited desirable compressive performance.[91a] Under longitudinal compression, the composites exhibited dramatic increase in stiffness over the entire strain range, and showed a longitudinal modulus of ~18.87 MPa between 0 and 8% strain, which was a 600% and 3300% increase as compared with the pure matrix and CNT array, respectively. Anisotropic characteristics and damping capability were also observed for such continuous aligned CNT composites. In order to prepare thin composite films for electrical conductivity testing, Peng et al. reported a method for preparing thin CNT composites by slicing a polymer-filtrated CNT array perpendicular[91a] or parallel[91b] to the array. Particularly, MWCNTs penetrated through the composite film with open ends when sliced along the perpendicular direction as shown in **Figure 10**A. Figure 10B shows an electrode fabricated using the composite film. The

  

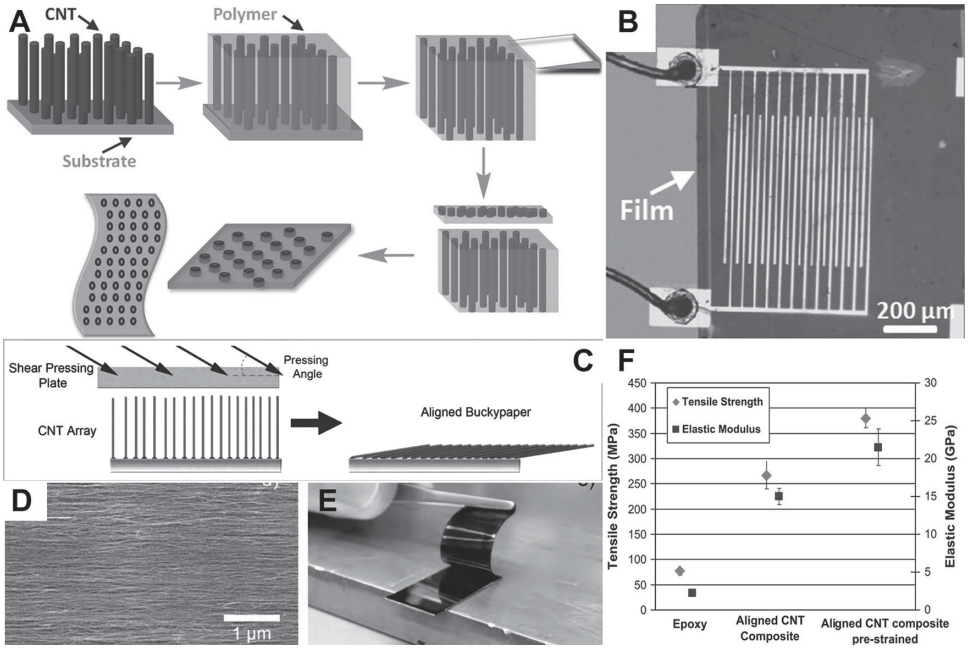


**Figure 10.** (A) Schematic of the preparation of perpendicularly aligned MWCNT/polymer films. (B) An electrode using MWCNT/polymer film as an ultrahigh sensor for NH3. Reproduced with permission.[91a] Copyright 2011, Wiley-VCH. (C) Schematic of the morphology of the array before and after shear pressing, (D) SEM image of the end of the preform showing the alignment of CNTs and (E) the aligned CNT preform is easily removed from the substrate by hand and ready for resin infusion. Reproduced with permission.[90e] Copyright 2010, Elsevier.

composite showed high sensitivity to $NH_3$ because of the open ends and the aligned structure. The composites could be transparent by choosing an appropriate polymer and film thickness. Moreover, the composites showed stable electrical resistance in response to repetitive bending. However, it is still a challenge to characterize the tensile properties along the nanotube direction owing to the size limitation of these samples.

In a recent report, instead of direct incorporation into polymer matrix, CNT arrays were "pushed down" to form aligned CNT buckypapers or films using a method first reported by Wang et al.,[97] followed by polymer infiltration (Figure 10C).[90e] CNTs were uniformly converted from their vertical orientation to a horizontal orientation after pushing (Figure 10D). Meanwhile, the packing density of CNTs was increased. After shear pressing,[88b] the aligned preforms were removed from the growth substrate (Figure 10E) and then soaked in an epoxy resin solution to form prepregged sheets. The dry CNT preforms exhibited a failure strength of 16 MPa, and the cured prepregs showed a tensile strength reaching 300 MPa and a modulus of 15 GPa. To further improve the mechanical properties of the composites by reducing CNT waviness, the resin infused prepregs were exposed to a strain of 5% before curing, followed by cutting the sheet into test strips and then curing. Such pre-cure-stretching increased the maximum tensile strength by 33% to 402 MPa and elastic modulus by 50% to 22.3 GPa as shown in Figure 10F These results demonstrate that straightening wavy CNTs can effectively improve the strength and stiffness of the composites.

In the shear pressing strategy, aligned CNT arrays containing long nanotubes can be converted into aligned CNT performs in seconds. The preforms meet the desired characteristics of millimeter long CNTs, high volume fraction, high degree of CNT alignment, and fast processing simultaneously. Additionally, the parallel alignment and through-the-thickness morphology of CNTs in the preforms facilitate resin infusion of the preform and thus create composites with both good unidirectional and through-the-thickness properties. However, one challenge of this strategy is to provide good resin infusion. Because the pushing and pressing processes remove the empty space between CNTs, many of the CNTs form much larger bundles. Bundling in turn reduces the effective reinforcement of the aligned CNTs in the composite due to less effective load transfer. Another limitation of this strategy is its inability to produce composite prepregs continuously and at a large scale.

### 4.2. Stretching MWCNT Films for Strong Composites

As mentioned in Section 2, FCCVD is an effective method to produce large-scale CNT films in which CNTs are randomly aligned. Post-treatment by simple stretching can make the CNTs well aligned as shown in **Figure 11**. The tensile strength and Young's modulus of a randomly dispersed CNT buckypaper were 205 MPa and 1.1 GPa, respectively. The tensile strength increased to 390 MPa, 508 MPa, and 668 MPa, which represent 90%, 148% and 226% improvements, after stretching 30%, 35% and 40%, respectively. Young's modulus and electrical conductivity exhibited a similar trend.[90a] In another work,[98] stepwise stretching and pressing (Figure 11A) drastically improved the CNT alignment and packing density of FCCVD-produced CNT sheets. As shown in Figure 11B, the CNT sheet with one-time stretching (30%) and pressing produced a tensile strength of 416 MPa and a

  

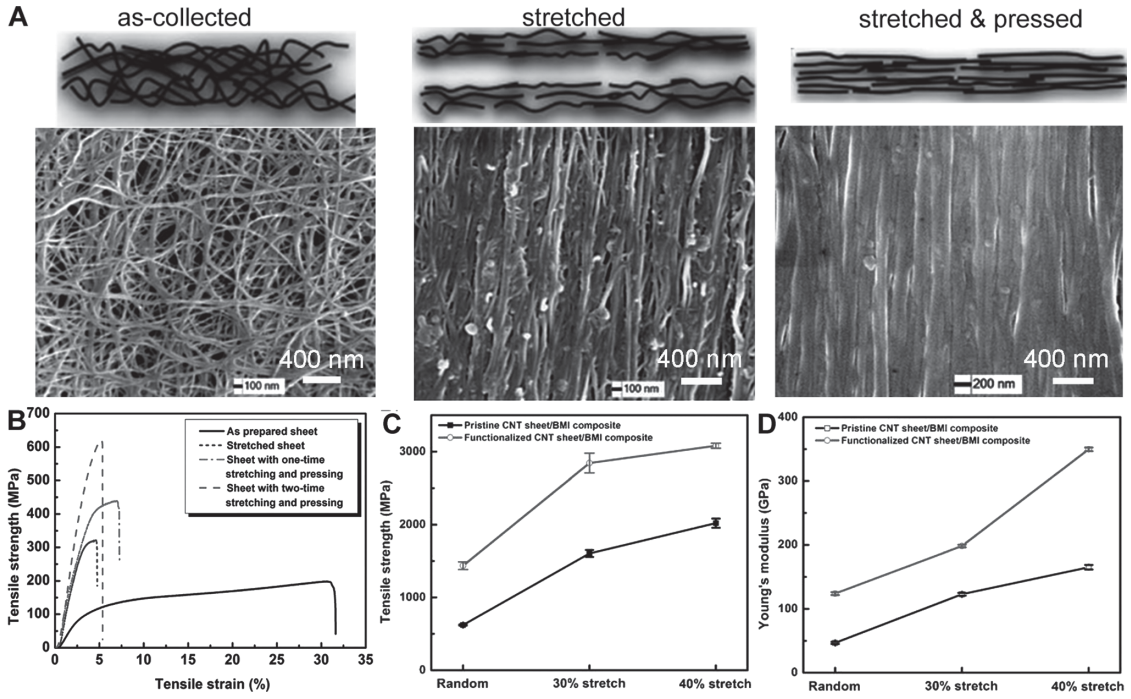


**Figure 11.** (A) Morphologies and (B) strain–stress curves of as-collected, stretched, and stretched and pressed CNT films. Reproduced with permission.[98] Copyright 2014, The Royal Society of Chemistry. (C) Comparisons of tensile strength and (D) Young's modulus measurements of the resultant composites with and without functionalization. Reproduced with permission.[90b] Copyright 2010, Wiley-VCH.

Young's modulus of 13.4 GPa, corresponding to 124% and 319% improvements, respectively, compared to the pristine CNT sheet. With additional 5% stretching and one more time pressing, the strength and modulus of the CNT sheet reached 598 MPa and 15.4 GPa, corresponding to 221% and 381% improvements, respectively. The CNT sheet after the second stretching and pressing obtained a high volume density of 0.98 g $cm^{-3}$ (increased by 109%).

Stretched CNT buckypaper (or sheet) can be incorporated into a polymer matrix to produce composites. After stretching, high weight fraction of aligned MWCNT buckypapers (60 wt%) was embedded in bismaleimide (BMI) matrix to form composites. The tensile strength and Young's modulus of the 30%-stretched CNT/BMI composite were 1.6 GPa and 122 GPa, respectively. When the stretch ratio increased to 40%, the tensile strength and Young's modulus reached 2.1 GPa and 169 GPa, respectively. The improvement of CNT alignment also gave rise to record-high electrical conductivity of 5,500 S $cm^{-1}$ for the 40%-stretched composites.

Aligned MWCNT buckypaper was functionalized to enable covalent bonding between the CNTs and the BMI resin matrix.[90b] Functionalization resulted in some degradation of the electrical conductivity of the composites. In contrast, functionalization led to further improvement in the mechanical properties of the composites (Figure 11, C and D). For example, for functionalized 40% stretched CNT-sheet/BMI nanocomposites, the tensile strength and Young's modulus reached up to 3.1 GPa and 350 GPa, respectively. This was the first report to demonstrate that the mechanical properties of CNT composites can exceed the state-of-the-art unidirectional carbon fiber composites.

### 4.3. Layered Assembly of Aligned CNT Films for Multifunctional Composites

CNT thin films drawn from spinnable arrays are of high purity and have good alignment compared to those synthesized by FCCVD. They are promising for fabricating high-performance composites. Three major strategies have been developed for fabricating composites based on such super-aligned MWCNT sheets. 1) Stacking and infiltrating strategy: polymer is infiltrated after single or multiple layers of aligned MWCNT sheet are assembled on a substrate. 2) Spraying-winding strategy: the as-drawn CNTs are continuously wound onto a rotating mandrel under the spray of a polymer solution. 3) Stretch-winding strategy: evolved from the spraying-winding method, this strategy enables the as-drawn CNTs to be further straightened before being incorporated into polymer matrix.

In the stacking and infiltrating strategy, CNT preforms were made by stacking multiple layers of CNT films and then infiltrating the aligned stacks with epoxy resin using a vacuum-assisted infiltration.[90c,99] This method produced composites with 16.5 wt% CNTs, which showed a tensile strength and Young's modulus of 231.5 MPa and 20.4 GPa, respectively. Polymers were also directly spin-coated or casted on as-drawn aligned CNT film supported by a substrate.[100] Monomers could also be introduced to the aligned MWCNT sheet, followed by in situ polymerization. This strategy utilized aligned CNTs and improved the resultant composite properties to some extent. However, the uniformity of infiltration is a challenge because the preforms are already tightly packed.

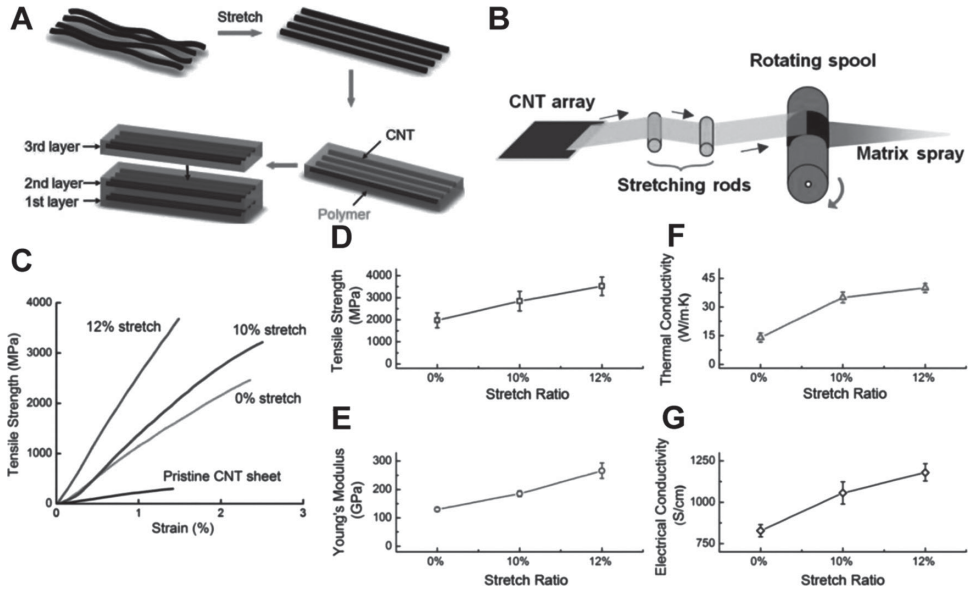


**Figure 12.** (A) Schematic illustration of the concept of straightening CNTs before embedding them in a polymer matrix in a layered fashion. (B) Schematic illustration of the experimental setup for the stretching-spraying-winding process. (C) Typical stress–strain curves of pristine CNT sheet, and composites with and without stretching, demonstrating a significant improvement of the mechanical properties through aligning and straightening of CNTs. Effect of stretching on (D) tensile strength and (E) Young's modulus, (F) thermal conductivity, and (G) electrical conductivity of the composites. Reproduced with permission.[35b] Copyright 2013, Francis and Taylor Group.

To tackle this issue, we used a spraying-winding strategy that produced well-dispersed CNT/polymer composites. As-drawn CNTs were continuously wound onto a rotating mandrel under the spray of a polymer solution.[35d] A wide variety of polymers including poly(vinyl alcohol) (PVA), nylon 6,6, epoxy, and polyimide have been studied. Typical spray-wound MWCNT/PVA composites exhibit a tensile strength of 1.8 GPa, Young's modulus of 40–96 GPa, toughness of 38–100 J $g^{-1}$ and electrical conductivity of 780 S $cm^{-1}$. Compared to regular infiltration methods that cannot avoid disturbance to CNT alignment due to migration of polymer molecules and flow of the liquid, the spraying–winding process deposits polymer onto each layer of well-aligned CNT films and maintains the aligned structure. Additionally, it allows the polymer matrix to penetrate between individual or very small bundles of CNTs instead of large bundles. Therefore, the CNTs or their bundles are integrated with the matrix at molecular level, which is critical for ensuring the effectiveness of load transfer, and thereby enhancing the mechanical properties of the resulting composites. Most importantly, this fabrication approach directly produces composite prepregs in one step, and the production rate depends on the rotation speed of the mandrel, and is thus conducive to large-scale productions.

One critical issue that prevents the full utilization of the reinforcing potential of the CNTs is the waviness of nanotubes. Micrographs show that individual nanotubes are wavy microscopically.[50] CNTs with different degrees of waviness do not carry applied load uniformly, cannot be packed densely, and have poor inter-tube connections, all of which adversely affect the strength, stiffness, and conductivity of the resulting CNT composites. The adverse effect of CNT waviness on composite properties has been clearly demonstrated by simulations.[101] We recently reported a stretching strategy to straighten wavy CNTs before embedding them into a polymer matrix during the spraying-winding processes (**Figure 12**A).[35b] The CNT film was stretched according to a stretch ratio $(L_S\text{-}L_0)/L_0$, where $L_S$ and $L_0$ are the length of the CNT film after and before stretching, respectively. CNT/bismaleimide composites, with a volume fraction of 46%, were fabricated by the stretch–winding approach and exhibited a combined strength and Young's modulus exceeding current carbon fiber reinforced polymer (CFRP) composites. The CNT composite that was stretched by 12% achieved a tensile strength of 3.8 GPa and Young's modulus of 293 GPa, as shown in Figure 12C–E. The average strength and stiffness of the CNT composites were 3.5 GPa and 266 GPa, respectively. The thermal conductivity was 41 W $m^{-1}$ $K^{-1}$ (Figure 12F) and the electrical conductivity was 1230 S·$cm^{-1}$ (Figure 12G). These results indicated that the stretching process increased their load carrying efficiency, and promoted a more efficient transfer of phonons and electrons along the CNT length direction of the composites by improving the alignment of CNTs.

As shown in Table 2, the CNTs for preparing composites have diameters of >10 nm. Considering that the outmost walls of CNTs play a dominant role in load transfer, large contact area between CNTs is of great importance for CNT films or fibers to achieve high strength. Small-diameter CNTs are superior because they have a large contact area in a unit volume compared to the large-diameter nanotubes. **Figure 13** (A–E) shows our results on preparing strong CNT films using small-diameter and few-walled CNTs. The CNTs contained 2–4 graphitic walls and have diameters of ~5 nm (Figure 13C). The preparation method was similar to the one used for composites.[35d] Instead of spraying polymers during winding, ethanol was sprayed to densify the CNT film. CNTs were densely packed in the films, which appears

  

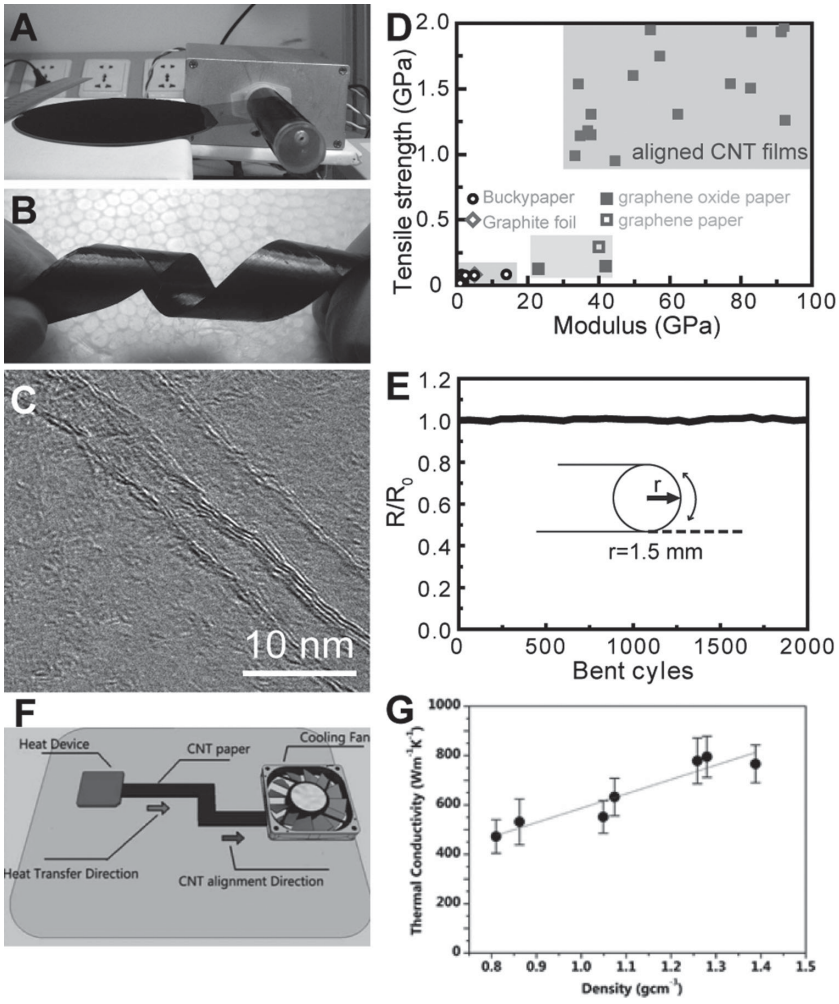


**Figure 13.** (A) Setup for winding aligned CNT films and (B) an as-prepared CNT film, (C) TEM image of few-walled CNTs. (D) Comparation of aligned CNT films in terms of tensile strength and modulus with the reported buckypapers, graphite foil, and graphene papers by wet chemistry methods. (E) Resistance change of a 6 μm-thick CNT film after the film was bent to a 1.5 mm radius more than 2000 times. Reproduced with permission.[11a] Copyright 2012, American Chemical Society. (G) Schematic of aligned CNT films as heat-transfer materials. (H) Thermal conductivities of CNT films as afunction of sample density. Reproduced with permission.[102] Copyright 2012, American Chemical Society.

a smooth and shinning surface as shown in Figure 13B. The films showed tensile strengths of 1.1–1.9 GPa and Young's modulus of 40–90 GPa (Figure 13D), which are markedly superior to other types of carbon-based films ever reported, including commercial graphite foils, buckypapers, and graphene related papers (Table 2). The films are strong but not brittle. They can bear severe bending (even being folded), and shows good structure integrity and negligible change in electric conductivity (Figure 13E). We are working on preparation of even stronger composites using the small-diameter CNTs and related results will be reported in a future publication. The good nanotube alignment makes the CNT films promising for directional heat transfer materials as demonstrated in Figure 13F. Zhang et al. reported high-density CNT films that have thermal conductivity up to 776 W $m^{-1}$ $K^{-1}$ in the direction of nanotube alignment.[102] They showed that the thermal conductivity increased with density as shown in Figure 13G. High thermal conductivity was achieved when the density of the aligned CNT films reached 1.39 g/$cm^3$.[102]

## 5. Summary

Dry processable CNTs not only simplify the fabrication of nanotube-based devices and composites but also improve their performance compared with CNTs processed by wet-solution-based methods. There is no doubt that the performance of nanotube-based functional devices and composites highly depend on the structure of nanotubes. Therefore, controlled growth of dry processable CNTs is of great importance. The existing issues on the growth of dry processable CNTs are listed as follows. For spinnable CNT arrays, 1) nanotubes are very defective as indicated by the low G/D Raman intensity ratio.[33,103] The defects decrease the mechanical properties and the thermal and electrical conductivities of the nanotubes and their assembly.[104] 2) CNTs typically show semi-metallic conductive properties at room temperature due to their relatively large diameter (5–80) nm and multi-walled structure,[9b,104,105] which are not suitable for electronics such as field effect transistors. Spinnable SWCNT arrays are therefore desirable not only for electronics but also for high-performance composites. 3) Other important issues include understanding the spinning mechanism of CNT arrays and optimizing array structures to improve spinnability. The challenges for CNT films prepapred by FCCVD method include 1) the poor uniformity of the nanotube films and 2) the removal of impurities such as catalyst and amorphous carbon.

Although aligned CNTs with superior mechanical and physical properties have been successfully developed, research on aligned CNT composites and devices is still in its infancy. Better understanding of multi-scale structure-property relationship for CNT materials needs to be established. This includes further study of the effect of CNT type, morphology and waviness at the nanoscale, the effect of CNT arrangement, alignment, intertube coupling and stress transfer at the microscale, and the effect of sheet arrangement at the macroscale on final material properties. Additionally, some challenges remain for the synthesis of high and consistent quality CNT arrays and the translation of unique properties of individual CNTs to macroscopic CNT assemblies. Further sustained efforts need to focus on realizing the full potential of CNTs in hierarchical structures, to enable future aerospace technologies and to inspire new devices that

NANO MICRO small

can capitalize on their unique properties. Finally, to commercialize dry-processable CNTs in future functional devices and composites, the greatest challenge is the large-scale production of CNTs with consistent and reproducible quality. This requires the precise control of synthesis parameters, which has been a challenge in most laboratories.

## Acknowledgements

*J. Di and X. Wang contributed equally to this work. This work was supported by the National Science Foundation of China (No.21203238), the National Basic Research Program (No. 2011CB932600-G), and Knowledge Innovation Program (KJCX2. YW.M12) of the Chinese Academy of Sciences. X.W. and Y.T.Z. are grateful for the financial support of US Air Force Office of Scientific Research (FA9550–12–1–0088 and FA9550–11–1–0124) and NASA Marshall Space Flight Center.*

[1] M. F. L. De Volder, S. H. Tawfick, R. H. Baughman, A. J. Hart, *Science* **2013**, *339*, 535.
[2] a) M.-F. Yu, O. Lourie, M. J. Dyer, K. Moloni, T. F. Kelly, R. S. Ruoff, *Science* **2000**, *287*, 637; b) B. Peng, M. Locascio, P. Zapol, S. Li, S. L. Mielke, G. C. Schatz, H. D. Espinosa, *Nat. Nanotechnol.* **2008**, *3*, 626; c) R. Zhang, Q. Wen, W. Qian, D. S. Su, Q. Zhang, F. Wei, *Adv. Mater.* **2011**, *23*, 3387; d) Min-Feng Yu, Bradley, S. Files, Sivaram Arepalli, a. R. S. Ruoff, *Phys. Rev. Lett.* **2000**, *84*, 4.
[3] A. Jorio, G. Dresselhaus, M. S. Dresselhaus, *Carbon Nanotubes: Advanced Topics in the Synthesis, Structure, Properties and Applications*Springer-Verlag, Berlin/Heidelberg/New York **2008**.
[4] L. Liu, W. Ma, Z. Zhang, *Small* **2011**, *7*, 1504.
[5] a) Z. Spitalsky, D. Tasis, K. Papagelis, C. Galiotis, *Prog. Polym. Sci.* **2010**, *35*, 357; b) D. Tasis, N. Tagmatarchis, A. Bianco, M. Prato, *Chem. Rev.* **2006**, *106*, 1105.
[6] M. D. Rossell, C. Kuebel, G. Ilari, F. Rechberger, F. J. Heiligtag, M. Niederberger, D. Koziej, R. Erni, *Carbon* **2013**, *61*, 404.
[7] J. Xu, T. S. Fisher, *Int. J. Heat Mass. Tran* **2006**, *49*, 1658.
[8] D. N. Futaba, K. Hata, T. Yamada, T. Hiraoka, Y. Hayamizu, Y. Kakudate, O. Tanaike, H. Hatori, M. Yumura, S. Iijima, *Nat. Mater.* **2006**, *5*, 987.
[9] a) K. L. Jiang, Q. Q. Li, S. S. Fan, *Nature* **2002**, *419*, 801; b) M. Zhang, S. Fang, A. A. Zakhidov, S. B. Lee, A. E. Aliev, C. D. Williams, K. R. Atkinson, R. H. Baughman, *Science* **2005**, *309*, 1215.
[10] K. Jiang, J. Wang, Q. Li, L. Liu, C. Liu, S. Fan, *Adv. Mater.* **2011**, *23*, 1154.
[11] a) J. Di, D. Hu, H. Chen, Z. Yong, M. Chen, Z. Feng, Y. Zhu, Q. Li, *ACS Nano* **2012**, *6*, 5457; b) X. F. Zhang, T. V. Sreekumar, T. Liu, S. Kumar, *J. Phys. Chem. B* **2004**, *108*, 16435; c) R. H. Baughman, C. Cui, A. A. Zakhidov, Z. Iqbal, J. N. Barisci, G. M. Spinks, G. G. Wallace, A. Mazzoldi, D. De Rossi, A. G. Rinzler, *Science* **1999**, *284*, 1340; d) N. A. Kumar, I. Y. Jeon, G. J. Sohn, R. Jain, S. Kumar, J. B. Baek, *ACS Nano* **2011**, *5*, 2324.
[12] W. Lu, M. Zu, J. H. Byun, B. S. Kim, T. W. Chou, *Adv. Mater.* **2012**, *24*, 1805.
[13] a) Z. Ren, Z. Huang, J. Xu, J. Wang, P. Bush, M. Siegal, P. Provencio, *Science* **1998**, *282*, 1105; b) S. Fan, M. G. Chapline, N. R. Franklin, T. W. Tombler, A. M. Cassell, H. Dai, *Science* **1999**, *283*, 512; c) K. Hata, D. N. Futaba, K. Mizuno, T. Namai, M. Yumura, S. Iijima, *Science* **2004**, *306*, 1362.
[14] a) H. Zhu, C. Xu, D. Wu, B. Wei, R. Vajtai, P. M. Ajayan, *Science* **2002**, *296*, 884; b) Y. L. Li, I. A. Kinloch, A. H. Windle, *Science* **2004**, *304*, 276.
[15] G. G. Tibbetts, D. W. Gorkiewicz, R. L. Alig, *Carbon* **1993**, *31*, 809.
[16] a) H. Cheng, F. Li, G. Su, H. Pan, L. He, X. Sun, M. Dresselhaus, *Appl. Phys. Lett.* **1998**, *72*, 3282; b) H. Cheng, F. Li, X. Sun, S. Brown, M. Pimenta, A. Marucci, G. Dresselhaus, M. Dresselhaus, *Chem. Phys. Lett.* **1998**, *289*, 602.
[17] L. Song, L. Ci, L. Lv, Z. Zhou, X. Yan, D. Liu, H. Yuan, Y. Gao, J. Wang, L. Liu, X. Zhao, Z. Zhang, X. Dou, W. Zhou, G. Wang, C. Wang, S. Xie, *Adv. Mater.* **2004**, *16*, 1529.
[18] Q. Liu, W. Ren, D.-W. Wang, Z.-G. Chen, S. Pei, B. Liu, F. Li, H. Cong, C. Liu, H.-M. Cheng, *ACS Nano* **2009**, *3*, 707.
[19] W. J. Ma, L. Song, R. Yang, T. H. Zhang, Y. C. Zhao, L. F. Sun, Y. Ren, D. F. Liu, L. F. Liu, J. Shen, Z. X. Zhang, Y. J. Xiang, W. Y. Zhou, S. S. Xie, *Nano Lett.* **2007**, *7*, 2307.
[20] P. Nikolaev, M. J. Bronikowski, R. K. Bradley, F. Rohmund, D. T. Colbert, K. Smith, R. E. Smalley, *Chem. Phys. Lett.* **1999**, *313*, 91.
[21] A. G. Nasibulin, A. Kaskela, K. Mustonen, A. S. Anisimov, V. Ruiz, S. Kivisto, S. Rackauskas, M. Y. Timmermans, M. Pudas, B. Aitchison, M. Kauppinen, D. P. Brown, O. G. Okhotnikov, E. I. Kauppinen, *ACS Nano* **2011**, *5*, 3214.
[22] a) S. Helveg, C. Lopez-Cartes, J. Sehested, P. L. Hansen, B. S. Clausen, J. R. Rostrup-Nielsen, F. Abild-Pedersen, J. K. Norskov, *Nature* **2004**, *427*, 426; b) M. Stadermann, S. P. Sherlock, J. B. In, F. Fornasiero, H. G. Park, A. B. Artyukhin, Y. M. Wang, J. J. De Yoreo, C. P. Grigoropoulos, O. Bakajin, A. A. Chernov, A. Noy, *Nano Lett.* **2009**, *9*, 738.
[23] a) W. Li, S. Xie, L. X. Qian, B. Chang, B. Zou, W. Zhou, R. Zhao, G. Wang, *Science* **1996**, *274*, 1701; b) Z. W. Pan, S. S. Xie, B. H. Chang, C. Y. Wang, L. Lu, W. Liu, W. Y. Zhou, W. Z. Li, L. X. Qian, *Nature* **1998**, *394*, 631.
[24] P. B. Amama, C. L. Pint, L. McJilton, S. M. Kim, E. A. Stach, P. T. Murray, R. H. Hauge, B. Maruyama, *Nano Lett.* **2008**, *9*, 44.
[25] D. Futaba, J. Goto, S. Yasuda, T. Yamada, M. Yumura, K. Hata, *Adv. Mater.* **2009**, *21*, 4811.
[26] a) T. de los Arcos, Z. M. Wu, P. Oelhafen, *Chem. Phys. Lett.* **2003**, *380*, 419; b) P. B. Amama, C. L. Pint, S. M. Kim, L. McJilton, K. G. Eyink, E. A. Stach, R. H. Hauge, B. Maruyama, *ACS Nano* **2010**, *4*, 895.
[27] a) Q. W. Li, X. F. Zhang, R. F. DePaula, L. X. Zheng, Y. H. Zhao, L. Stan, T. G. Holesinger, P. N. Arendt, D. E. Peterson, Y. T. Zhu, *Adv. Mater.* **2006**, *18*, 3160; b) S. Yasuda, D. N. Futaba, T. Yamada, J. Satou, A. Shibuya, H. Takai, K. Arakawa, M. Yumura, K. Hata, *ACS Nano* **2009**, *3*, 4164; c) A. A. Puretzky, G. Eres, C. M. Rouleau, I. N. Ivanov, D. B. Geohegan, *Nanotechnology* **2008**, *19*, 055605; d) K. Hasegawa, S. Noda, *ACS Nano* **2011**, *5*, 975.
[28] R. Guzman de Villoria, S. L. Figueredo, A. J. Hart, S. A. Steiner 3rd, A. H. Slocum, B. L. Wardle, *Nanotechnology* **2009**, *20*, 405611.
[29] R. Guzmán de Villoria, A. J. Hart, B. L. Wardle, *ACS Nano* **2011**, *5*, 4850.
[30] K. Liu, Y. H. Sun, L. Chen, C. Feng, X. F. Feng, K. L. Jiang, Y. G. Zhao, S. S. Fan, *Nano Lett.* **2008**, *8*, 700.
[31] M. Zhang, K. R. Atkinson, R. H. Baughman, *Science* **2004**, *306*, 1358.
[32] a) X. B. Zhang, K. L. Jiang, C. Teng, P. Liu, L. Zhang, J. Kong, T. H. Zhang, Q. Q. Li, S. S. Fan, *Adv. Mater.* **2006**, *18*, 1505; b) C. P. Huynh, S. C. Hawkins, *Carbon* **2010**, *48*, 1105; c) J.-H. Kim, H.-S. Jang, K. H. Lee, L. J. Overzet, G. S. Lee, *Carbon* **2010**, *48*, 538; d) J. Di, Z. Yong, X. Yang, Q. Li, *Appl. Surf. Sci.* **2011**, *258*, 13.
[33] J. Di, Z. Yong, X. Zheng, B. Sun, Q. Li, *Small* **2013**, *9*, 1367.

  

[34] Y. Inoue, K. Kakihata, Y. Hirono, T. Horie, A. Ishida, H. Mimura, *Appl. Phys. Lett.* **2008**, *92*, 213113.
[35] a) J. Jia, J. Zhao, G. Xu, J. Di, Z. Yong, Y. Tao, C. Fang, Z. Zhang, X. Zhang, L. Zheng, Q. Li, *Carbon* **2011**, *49*, 1333; b) X. Wang, Z. Z. Yong, Q. W. Li, P. D. Bradford, W. Liu, D. S. Tucker, W. Cai, H. Wang, F. G. Yuan, Y. T. Zhu, *Mater. Res. Lett.* **2013**, *1*, 19; c) W. Liu, H. Zhao, Y. Inoue, X. Wang, P. D. Bradford, H. Kim, Y. Qiu, Y. Zhu, *Composites Part A* **2012**, *43*, 587; d) W. Liu, X. Zhang, G. Xu, P. D. Bradford, X. Wang, H. Zhao, Y. Zhang, Q. Jia, F.-G. Yuan, Q. Li, Y. Qiu, Y. Zhu, *Carbon* **2011**, *49*, 4786.
[36] L. Liu, S. Fan, *J. Am. Chem. Soc.* **2001**, *123*, 11502.
[37] A. Fallah Gilvaei, K. Hirahara, Y. Nakayama, *Carbon* **2011**, *49*, 4928.
[38] C. Zhu, C. Cheng, Y. H. He, L. Wang, T. L. Wong, K. K. Fung, N. Wang, *Carbon* **2011**, *49*, 4996.
[39] A. A. Kuznetsov, A. F. Fonseca, R. H. Baughman, A. A. Zakhidov, *ACS Nano* **2011**, *5*, 985.
[40] a) M. Xu, D. N. Futaba, M. Yumura, K. Hata, *ACS Nano* **2012**, *6*, 5837; b) G. Zhong, J. H. Warner, M. Fouquet, A. W. Robertson, B. Chen, J. Robertson, *ACS Nano* **2012**, *6*, 2893.
[41] a) A. Kumar, C. Zhou, *ACS Nano* **2010**, *4*, 11; b) L. Hu, D. S. Hecht, G. Grüner, *Chem. Rev.* **2010**, *110*, 5790.
[42] Z. Wu, Z. Chen, X. Du, J. M. Logan, J. Sippel, M. Nikolou, K. Kamaras, J. R. Reynolds, D. B. Tanner, A. F. Hebard, A. G. Rinzler, *Science* **2004**, *305*, 1273.
[43] B. Dan, G. C. Irvin, M. Pasquali, *ACS Nano* **2009**, *3*, 835.
[44] F. Mirri, A. W. K. Ma, T. T. Hsu, N. Behabtu, S. L. Eichmann, C. C. Young, D. E. Tsentalovich, M. Pasquali, *ACS Nano* **2012**, *6*, 9737.
[45] N. Saran, K. Parikh, D.-S. Suh, E. Muñoz, H. Kolla, S. K. Manohar, *J. Am. Chem. Soc.* **2004**, *126*, 4462.
[46] J. K. W. Sandler, A. H. Windle, C. A. Martin, M. L. Schwarz, W. Bauhofer, K. Schulte, M. S. P. Shaffer, *Continuous Nanophase and Nanostructured Materials* **2004**, *788*, 221.
[47] a) A. Kaskela, A. G. Nasibulin, M. Y. Timmermans, B. Aitchison, A. Papadimitratos, Y. Tian, Z. Zhu, H. Jiang, D. P. Brown, A. Zakhidov, E. I. Kauppinen, *Nano Lett.* **2010**, *10*, 4349; b) G.-H. Xu, J.-Q. Huang, Q. Zhang, M.-Q. Zhao, F. Wei, *Appl. Phys. A* **2011**, *103*, 403; c) Z. Li, Y. Jia, J. Wei, K. Wang, Q. Shu, X. Gui, H. Zhu, A. Cao, D. Wu, *J. Mater. Chem.* **2010**, *20*, 7236.
[48] J. W. Jo, J. W. Jung, J. U. Lee, W. H. Jo, *ACS Nano* **2010**, *4*, 5382.
[49] C. Feng, K. Liu, J.-S. Wu, L. Liu, J.-S. Cheng, Y. Zhang, Y. Sun, Q. Li, S. Fan, K. Jiang, *Adv. Funct. Mater.* **2010**, *20*, 885.
[50] Y. Zhang, C. J. Sheehan, J. Zhai, G. Zou, H. Luo, J. Xiong, Y. T. Zhu, Q. X. Jia, *Adv. Mater.* **2010**, *22*, 3027.
[51] F. Xu, X. Wang, Y. Zhu, Y. Zhu, *Adv. Funct. Mater.* **2012**, *22*, 1279.
[52] K. Liu, Y. Sun, P. Liu, X. Lin, S. Fan, K. Jiang, *Adv. Funct. Mater.* **2011**, *21*, 2721.
[53] J. Wei, Y. Jia, Q. Shu, Z. Gu, K. Wang, D. Zhuang, G. Zhang, Z. Wang, J. Luo, A. Cao, D. Wu, *Nano Lett.* **2007**, *7*, 2317.
[54] Y. Jia, J. Wei, K. Wang, A. Cao, Q. Shu, X. Gui, Y. Zhu, D. Zhuang, G. Zhang, B. Ma, L. Wang, W. Liu, Z. Wang, J. Luo, D. Wu, *Adv. Mater.* **2008**, *20*, 4594.
[55] P. Wadhwa, B. Liu, M. A. McCarthy, Z. Wu, A. G. Rinzler, *Nano Lett.* **2010**, *10*, 5001.
[56] Y. Jung, X. Li, N. K. Rajan, A. D. Taylor, M. A. Reed, *Nano Lett.* **2012**, *13*, 95.
[57] Y. Jia, A. Cao, X. Bai, Z. Li, L. Zhang, N. Guo, J. Wei, K. Wang, H. Zhu, D. Wu, P. M. Ajayan, *Nano Lett.* **2011**, *11*, 1901.
[58] H.-Z. Geng, K. K. Kim, K. P. So, Y. S. Lee, Y. Chang, Y. H. Lee, *J. Am. Chem. Soc.* **2007**, *129*, 7758.
[59] a) Y. Jia, A. Cao, F. Kang, P. Li, X. Gui, L. Zhang, E. Shi, J. Wei, K. Wang, H. Zhu, D. Wu, *Phys. Chem. Chem. Phys.* **2012**, *14*, 8391; b) Y. Jia, P. Li, X. Gui, J. Wei, K. Wang, H. Zhu, D. Wu, L. Zhang, A. Cao, Y. Xu, *Appl. Phys. Lett.* **2011**, *98*, 133115.
[60] E. Shi, L. Zhang, Z. Li, P. Li, Y. Shang, Y. Jia, J. Wei, K. Wang, H. Zhu, D. Wu, S. Zhang, A. Cao, *Sci. Rep.* **2012**, *2*, 884.
[61] Y. Jia, P. Li, J. Wei, A. Cao, K. Wang, C. Li, D. Zhuang, H. Zhu, D. Wu, *Mater. Res. Bull.* **2010**, *45*, 1401.
[62] M. Grätzel, *Nature* **2001**, *414*, 338.
[63] F. Hao, Z. Wang, Q. Luo, J. Lou, J. Li, J. Wang, S. Fan, K. Jiang, H. Lin, *J. Mater. Chem.* **2012**, *22*, 22756.
[64] K. Aitola, J. Halme, S. Feldt, P. Lohse, M. Borghei, A. Kaskela, A. G. Nasibulin, E. I. Kauppinen, P. D. Lund, G. Boschloo, A. Hagfeldt, *Electrochim. Acta* **2013**, *111*, 206.
[65] Z. Yang, T. Chen, R. He, G. Guan, H. Li, L. Qiu, H. Peng, *Adv. Mater.* **2011**, *23*, 5436.
[66] J. Di, Z. Yong, Z. Yao, X. Liu, X. Shen, B. Sun, Z. Zhao, H. He, Q. Li, *Small* **2013**, *9*, 148.
[67] a) L. Shen, C. Yuan, H. Luo, X. Zhang, K. Xu, F. Zhang, *J. Mater. Chem.* **2011**, *21*, 761; b) F.-F. Cao, Y.-G. Guo, S.-F. Zheng, X.-L. Wu, L.-Y. Jiang, R.-R. Bi, L.-J. Wan, J. Maier, *Chem. Mater.* **2010**, *22*, 1908.
[68] J. A. Lee, M. K. Shin, S. H. Kim, S. J. Kim, G. M. Spinks, G. G. Wallace, R. Ovalle-Robles, M. D. Lima, M. E. Kozlov, R. H. Baughman, *ACS Nano* **2011**, *6*, 327.
[69] H. Lin, L. Li, J. Ren, Z. Cai, L. Qiu, Z. Yang, H. Peng, *Sci. Rep.* **2013**, *3*, 1353.
[70] a) R. Zhou, C. Meng, F. Zhu, Q. Li, C. Liu, S. Fan, K. Jiang, *Nanotechnology* **2010**, *21*, 345701; b) J.-H. Kim, K. H. Lee, L. J. Overzet, G. S. Lee, *Nano Lett.* **2011**, *11*, 2611.
[71] Y. Wu, Y. Wei, J. Wang, K. Jiang, S. Fan, *Nano Lett.* **2013**, *13*, 818.
[72] K. Wang, S. Luo, Y. Wu, X. He, F. Zhao, J. Wang, K. Jiang, S. Fan, *Adv. Funct. Mater.* **2013**, *23*, 846.
[73] K. Fu, O. Yildiz, H. Bhanushali, Y. Wang, K. Stano, L. Xue, X. Zhang, P. D. Bradford, *Adv. Mater.* **2013**, *25*, 5109.
[74] H.-X. Zhang, C. Feng, Y.-C. Zhai, K.-L. Jiang, Q.-Q. Li, S.-S. Fan, *Adv. Mater.* **2009**, *21*, 2299.
[75] H. Lin, L. Li, J. Ren, Z. Cai, L. Qiu, Z. Yang, H. Peng, *Sci Rep* **2013**, *3*, 1353.
[76] C. Yu, C. Masarapu, J. Rong, B. Wei, H. Jiang, *Adv. Mater.* **2009**, *21*, 4793.
[77] A. E. Aliev, J. Oh, M. E. Kozlov, A. A. Kuznetsov, S. Fang, A. F. Fonseca, R. Ovalle, M. D. Lima, M. H. Haque, Y. N. Gartstein, M. Zhang, A. A. Zakhidov, R. H. Baughman, *Science* **2009**, *323*, 1575.
[78] L. Xiao, Z. Chen, C. Feng, L. Liu, Z. Q. Bai, Y. Wang, L. Qian, Y. Y. Zhang, Q. Q. Li, K. L. Jiang, S. S. Fan, *Nano Lett.* **2008**, *8*, 4539.
[79] A. E. Aliev, M. D. Lima, S. Fang, R. H. Baughman, *Nano Lett.* **2010**, *10*, 2374.
[80] Y. Wei, X. Lin, K. Jiang, P. Liu, Q. Li, S. Fan, *Nano Lett.* **2013**, *13*, 4795.
[81] L. Zhang, C. Feng, Z. Chen, L. Liu, K. Jiang, Q. Li, S. Fan, *Nano Lett.* **2008**, *8*, 2564.
[82] P. Liu, L. Liu, Y. Wei, K. Liu, Z. Chen, K. Jiang, Q. Li, S. Fan, *Adv. Mater.* **2009**, *21*, 3563.
[83] C. D. Williams, R. O. Robles, M. Zhang, S. Li, R. H. Baughman, A. A. Zakhidov, *Appl. Phys. Lett.* **2008**, *93*, 183506.
[84] Y. Sun, K. Liu, J. Miao, Z. Wang, B. Tian, L. Zhang, Q. Li, S. Fan, K. Jiang, *Nano Lett.* **2010**, *10*, 1747.
[85] Y. Zhu, X. Zhang, R. Li, Q. Li, *Sci. Rep.* **2014**, *4*, 4728.
[86] Y. Koo, R. Malik, N. Alvarez, L. White, V. N. Shanov, M. Schulz, B. Collins, J. Sankar, Y. Yun, *RSC Advances* **2014**, *4*, 16362.
[87] C. Park, J. Wilkinson, S. Banda, Z. Ounaies, K. E. Wise, G. Sauti, P. T. Lillehei, J. S. Harrison, *Polymer* **2006**, *44*, 1751.
[88] a) S. B. Kharchenko, J. F. Douglas, J. Obrzut, E. A. Grulke, K. B. Migler, *Nat. Mater.* **2004**, *3*, 564; b) N. Wada, Y. A. Kim, Y. Gotoh, M. Endo, T. Hayashi, *J. Seiyama54*, **2006**, 31; c) B. Z. Tang, H. Xu, *Macromolecules* **1999**, *32*, 2569.
[89] a) Y. Mai, X. Xie, X. Zhou, *49*, **2005**, 89; b) Z. Jia, Z. Wang, C. Xu, J. Liang, B. Wei, D. Wu, S. Zhu, *Mater. Sci. Engin. A* **1999**, *271*, 395; c) B. S. Shim, J. Zhu, E. Jan, K. Critchley, S. S. Ho, P. Podsiadlo, K. Sun, N. A. Kotov, *ACS Nano* **2009**, *3*, 1711;

  

d) J. Zhu, J. Kim, H. Peng, J. L. Margrave, V. N. Khabashesku, E. V. Barrera, *Nano Lett.* **2003**, *3*, 1107.
[90] a) Q. F. Cheng, J. W. Bao, J. Park, Z. Y. Liang, C. Zhang, B. Wang, *Adv. Funct. Mater.* **2009**, *19*, 3219; b) Q. F. Cheng, B. Wang, C. Zhang, Z. Y. Liang, *Small* **2010**, *6*, 763; c) Q. F. Cheng, J. P. Wang, J. J. Wen, C. H. Liu, K. L. Jiang, Q. Q. Li, S. S. Fan, *Carbon* **2010**, *48*, 260; d) Y. Inoue, Y. Suzuki, Y. Minami, J. Muramatsu, Y. Shimamura, K. Suzuki, A. Ghemes, M. Okada, S. Sakakibara, H. Mimura, K. Naito, *Carbon* **2011**, *49*, 2437; e) P. D. Bradford, X. Wang, H. Zhao, J.-P. Maria, Q. Jia, Y. T. Zhu, *Compos. Sci. Technol.* **2010**, *70*, 1980.
[91] a) L. Ci, J. Suhr, V. Pushparaj, X. Zhang, P. M. Ajayan, *Nano Lett.* **2008**, *8*, 2762; b) S. Huang, L. Li, Z. Yang, L. Zhang, H. Saiyin, T. Chen, H. Peng, *Adv. Mater.* **2011**, *23*, 47070; c) X. Sun, T. Chen, Z. Yang, H. Peng, *Accounts. Chem. Res.* **2012**, *46*, 539.
[92] H. Peng, M. Jain, Q. Li, D. E. Peterson, Y. Zhu, Q. Jia, *J. Am. Chem. Soc.* **2008**, *130*, 1130.
[93] X. Wang, P. D. Bradford, W. Liu, H. Zhao, Y. Inoue, J.-P. Maria, Q. Li, F.-G. Yuan, Y. Zhu, *Compos. Sci. Technol.* **2011**, *71*, 1677.
[94] A. Cao, P. L. Dickrell, W. G. Sawyer, M. N. Ghasemi-Nejhad, P. M. Ajayan, *Science* **2005**, *310*, 1307.
[95] J. Suhr, P. Victor, L. Ci, S. Sreekala, X. Zhang, O. Nalamasu, P. M. Ajayan, *Nature Nanotechnol.* **2007**, *2*, 417.
[96] L. Li, Z. Yang, H. Gao, H. Zhang, J. Ren, X. Sun, T. Chen, H. G. Kia, H. Peng, *Adv. Mater.* **2011**, *23*, 3730.
[97] D. Wang, P. C. Song, C. H. Liu, W. Wu, S. S. Fan, *Nanotechnology* **2008**, *19*, 075609.
[98] Q. Liu, M. Li, Y. Gu, Y. Zhang, S. Wang, Q. Li, Z. Zhang, *Nanoscale* **2014**, *6*, 4338.
[99] Q. Cheng, J. Wang, Q. Li, K. Jiang, S. Fan, *J. Mater. Res. 23*, **2008**, 2975.
[100] H. Peng, *J. Am. Chem. Soc.* **2008**, *130*, 42.
[101] a) F. Fisher, *Compos. Sci. and Technol. 63*, **2003**, 1689; b) F. Deng, Q.-S. Zheng, L.-F. Wang, C.-W. Nan, *Appl. Phys. Lett.* **2007**, *90*, 021914.
[102] L. Zhang, G. Zhang, C. Liu, S. Fan, *Nano Lett.* **2012**, *12*, 4848.
[103] a) J. Zhao, X. Zhang, J. Di, G. Xu, X. Yang, X. Liu, Z. Yong, M. Chen, Q. Li, *Small* **2010**, *6*, 2612; b) Y. Y. Zhang, G. F. Zou, S. K. Doorn, H. Htoon, L. Stan, M. E. Hawley, C. J. Sheehan, Y. T. Zhu, Q. X. Jia, *ACS Nano* **2009**, *3*, 2157.
[104] J.-H. Pöhls, M. B. Johnson, M. A. White, R. Malik, B. Ruff, C. Jayasinghe, M. J. Schulz, V. Shanov, *Carbon* **2012**, *50*, 4175.
[105] Q. Li, X. Zhang, S. B. Chikkannanavar, Y. Zhao, A. M. Dangelewicz, L. Zheng, S. K. Doorn, Q. Jia, D. E. Peterson, P. N. Arendt, Y. Zhu, *Adv. Mater.* **2007**, *19*, 3358.
[106] U. Dettlaff-Weglikowska, V. Skákalová, R. Graupner, S. H. Jhang, B. H. Kim, H. J. Lee, L. Ley, Y. W. Park, S. Berber, D. Tománek, S. Roth, *J. Am. Chem. Soc.* **2005**, *127*, 5125.
[107] S. Wang, Z. Liang, B. Wang, C. Zhang, *Adv. Mater.* **2007**, *19*, 1257.
[108] S. Malik, H. Rosner, F. Hennrich, A. Bottcher, M. M. Kappes, T. Beck, M. Auhorn, *Phys. Chem. Chem. Phys.* **2004**, *6*, 3540.
[109] I. W. Peter Chen, R. Liang, H. Zhao, B. Wang, C. Zhang, *Nanotechnology* **2011**, *22*, 485708.
[110] W.-T. Hong, N.-H. Tai, *Diam. Relat. Mater.* **2008**, *17*, 1577.
[111] H. Chen, M. Chen, J. Di, G. Xu, H. Li, Q. Li, *J. Phys. Chem. C* **2012**, *116*, 3903.
[112] J. E. Fischer, W. Zhou, J. Vavro, M. C. Llaguno, C. Guthy, R. Haggenmueller, M. J. Casavant, D. E. Walters, R. E. Smalley, *J. Appl. Phys.* **2003**, *93*, 2157.
[113] G. H. Xu, Q. Zhang, W. P. Zhou, J. Q. Huang, F. Wei, *Appl. Phys. A: Mater. Sci. Process.* **2008**, *92*, 531.
[114] J. N. Coleman, M. Cadek, R. Blake, V. Nicolosi, K. P. Ryan, C. Belton, A. Fonseca, J. B. Nagy, Y. K. Gun'ko, W. J. Blau, *Adv. Funct. Mater.* **2004**, *14*, 791.
[115] M. Cadek, J. N. Coleman, V. Barron, K. Hedicke, W. J. Blau, *Appl. Phys. Lett.* **2002**, *81*, 5123.
[116] R. E. Gorga, R. E. Cohen, *J. Polym. Sci., Part B: Polym. Phys.* **2004**, *42*, 2690.
[117] I. Y. Phang, L. Shen, S. Y. Chow, W.-D. Zhang, *Macromolecules* **2004**, *37*, 7214.
[118] M. A. Manchado, L. Valentini, J. Biagiotti, J. M. Kenny, *Carbon* **2005**, *43*, 1499.
[119] K. Yang, M. Gu, Y. Guo, X. Pan, G. Mu, *Carbon* **2009**, *47*, 1723.
[120] T. Morishita, M. Matsushita, Y. Katagiri, K. Fukumori, *J. Mater. Chem.* **2011**, *21*, 5610.
[121] A. Moisala, Q. Li, I. A. Kinloch, A. H. Windle, *Compos. Sci. Technol.* **2006**, *66*, 1285.
[122] Q. Cheng, M. Li, L. Jiang, Z. Tang, *Adv. Mater.* **2012**, *24*, 1838.
[123] Q. Jiang, X. Wang, Y. Zhu, D. Hui, Y. Qiu, *Composites Part B* **2014**, *56*, 408.

Received: May 25, 2014
Revised: July 1, 2014
Published online: August 13, 2014